Analysis of Vestibular Hair Cell Bundle Mechanics Using Finite Element Modeling

Joseph Allan Silber

Thesis submitted to the faculty of the
Virginia Polytechnic Institute and State University
in partial fulfillment of the requirements for the degree of

MASTER OF SCIENCE

in

Engineering Mechanics

J.Wallace Grant, Chair
Ellengene H. Peterson
John R. Cotton

November 18, 2002
Blacksburg, Virginia

Keywords: Vestibular System, Hair Cell, Finite Element

Analysis of Vestibular Hair Cell Bundle Mechanics Using Finite Element Modeling

by
Joseph Allan Silber
Committee Chairman: J.W. Grant
Engineering Mechanics

(ABSTRACT)

The vestibular system of vertebrates consists of the utricle, saccule, and the semicircular canals. Head movement causes deformation of hair cell bundles in these organs, which translate this mechanical stimulus into an electrical response sent to the nervous system.

This study consisted of two sections, both utilizing a Fortran-based finite element program to study hair cell bundle response. In the first part, the effects of variations in geometry and material properties on bundle mechanical response were studied. Six real cells from the red eared slider turtle utricle were modeled and their response to a gradually increased point load was analyzed. Bundle stiffness and tip link tension distributions were the primary data examined.

The cells fell into two groups based on stiffness. All cells exhibited an increase in stiffness as the applied load was increased, but cells in the stiffer group showed a greater increase. Tip link tensions in the compliant group were approximately 3 times as high as those in the stiffer group. Cells in the stiffer group were larger, with more cilia, and also had a higher stereocilia/kinocilium height ratio than the cells in the other group. The stereocilia/kinocilium height ratio was the most important geometric factor in influencing bundle stiffness. Modeling a bundle as just its middle row of stereocilia resulted in some decrease in stiffness, but more significantly, a stiffness that was virtually constant as applied load increased. Tip link tension distributions showed serial behavior in the core rows of stereocilia and parallel behavior in the outer rows; this trend intensified if the tip link elastic modulus was increased. It was demonstrated that full three-dimensional modeling of bundles is critical for obtaining complete and accurate results.

In the second part of the study, tip link ion gates were modeled. Sufficient tension in a tip link caused that link's ion gate to open, increasing the length of the link and causing its tension to decrease or the link to go slack. The two parameters that were varied were tip link elastic modulus and tip link gating distance d (change in length of the link). Bundle stiffness drops of up to 25% were obtained, but only when tip links went slack after gate opening; tip link slackening was dependent on tip link gating distance. Higher tip link modulus resulted in higher stiffness drops. Variable tip link modulus and tip link pre-tensioning were modeled. Variable tip link modulus resulted in increased bundle stiffness, especially under high applied loads, and in some cases, resulted in greater bundle stiffness drops when ion gates opened. Tip link pre-tensioning had no noticeable effect on bundle response. No evidence against inclusion of pre-tensioning or variable tip link elastic modulus was found.

ACKNOWLEDGEMENTS

I would like to thank first and foremost Dr. J.W. Grant, my advisor and committee chair, for all his assistance and guidance, both in this research and in my graduate studies in general. He's always been willing to give help above and beyond what is expected or required, and he made this whole process much easier than it would otherwise have been.

Also, I'd like to thank Dr. John Cotton for answering my many questions regarding Unix, Fortran, and his prior work, and for providing his thoughts on interpretation of data and results, as well as for agreeing to serve on my committee on short notice.

Thanks also to Dr. Peterson, for her collaboration and work on the biological aspect of the research of which this thesis is a part, and for taking time out of her busy schedule to be on my committee.

I'd also like to thank Jen Silverman for her help answering my questions regarding the thesis defense process, having gone through it only a few months before I did.

Finally, thanks as always to my wife and parents, for their continual support and encouragement.

TABLE OF CONTENTS

LIST OF FIGURES

LIST OF TABLES

CHAPTER 1: INTRODUCTION AND BACKGROUND

Balance, eye movement coordination, and posture all require feedback from the body on the position, orientation, and movement of various parts of the body. The vestibular system, located in the inner ear, plays a crucial role in these tasks by providing the brain with information on the orientation and motion of the skull.

The organs of the vestibular system are located in part of the membranous labyrinth portion of the inner ear. The components of this system are the three semicircular canals, which detect angular movement, and the utricle and saccule, which detect orientation and linear movement. Movement of the head, or a change in orientation of the head with respect to gravity, causes a mechanical deformation of receptor cells inside these organs. The receptor cells, called hair cells, translate this mechanical stimulus into an electrical response sent to the nervous system, a process explained in more detail below.

The Semicircular Canals

The three fluid-filled semicircular canals are mutually orthogonal, and can thus detect an angular acceleration about any axis. They are sensitive enough to measure accelerations as small as 0.1 $^{o}/sec^{2}$ (Kelly, 1991).

Receptor cells inside the semicircular canals are located in a thickened zone of epithelium known as the ampullary crest. A gel-like blob called the cupula fills the space above the ampullary crest. Stereocilia from receptor hair cells located on the crest stick up into the cupula. When the head rotates, the force exerted by the inertia of the fluid acts on and distorts the cupula, which in turn deforms the hair cells it is in contact with. This mechanical stimulus causes the hair cells to adjust their signals to the nervous system accordingly.

The Otolith Organs

The utricle and the saccule are known as the otolith organs. Receptor cells in the otolith organs are located in the macula, a thickened region equivalent to the ampullary crest. Above the macula, hair cells project into a gel layer that is in turn covered with a

layer of tiny calcium carbonate crystals known as otoconia. Linear movement of the head causes the otoconia to lag behind due to their inertia, and they exert a shear force on the gel layer, deforming the hair cells. Similarly, if the head is tilted, the denser otoconia will deflect towards the ground, causing shear.

Hair Cells: Anatomy

Hair cells are the basic sensory units in all of these vestibular organs. The cell body of a hair cell is sunk into the surrounding epithelium; the portion that protrudes is referred to as the hair cell bundle. The cell body is surrounded by supporting cells and is innervated by one or more vestibular ganglion cells, allowing the hair cell to communicate with the nervous system. Hair cells are categorized into two types. Type I hair cells have a flask-shaped body and are innervated by only one afferent nerve; Type II cells are more common, have a more cylindrical-shaped body, and are generally innervated by both afferent and efferent nerves.

The hair cell bundle is composed of approximately 10 to 100 or more "hairs" (Cotton, 1998). There are two types of "hairs" in a cell bundle: stereocilia and kinocilia, although there is generally only one kinocilium. The kinocilium is usually the tallest "hair" in a cell bundle. A key difference between a kinocilium and a stereocilium is structural. Stereocilia are not true cilia, and are in fact composed of thousands of actin filaments covered by a membrane. In contrast, kinocilia are true cilia and do not contain actin filaments, but are rather composed of a microtubular structure with 9 pairs of microtubules in a circle, sometimes surrounding 1 or 2 microtubules in the center ("9+1" or "9+2" configurations) (Lewis, et al.,1985). There are other differences between stereocilia and kinocilia as well. The stereocilia arise from an underlying structure called the cuticular plate, into which they are anchored; the kinocilium is not attached to the cuticular plate (Lewis, et al. 1985). Near the base of a stereocilium, the number of filaments decreases and the stereocilium tapers to a blunted cone shape. Because of the stiffness of the actin filaments, the stereocilia tend to pivot at their base when deflected, rather than bend smoothly. (Leish, et al., 1999). The actin filaments connect the cilia with the underlying cell body. As the stereocilia bends, the actin filaments slide past each

other in shear. In contrast, the kinocilium is about 15-20% thicker than the stereocilia, and does not taper. Figure 1.1 shows an electron micrograph of some hair cell bundles.

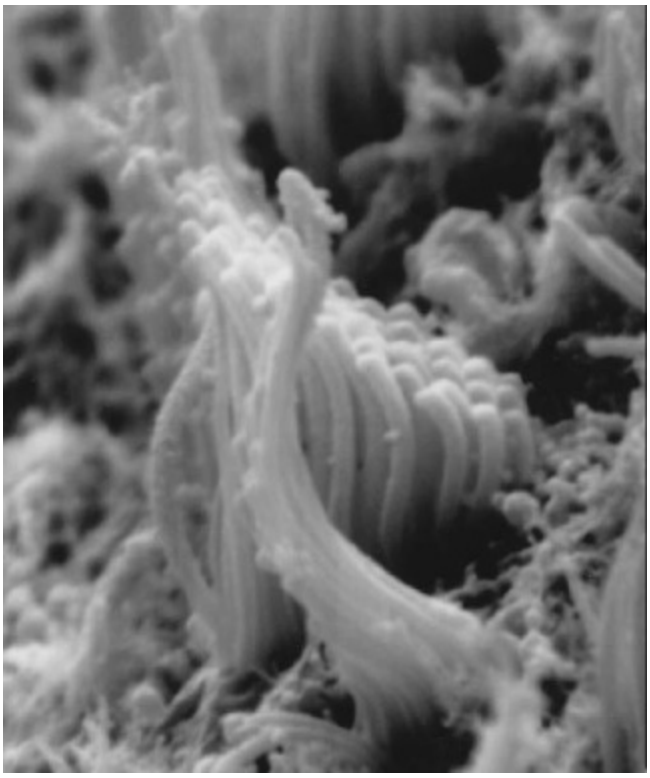

Figure 1.1: Scanning EM of hair cell bundles (Peterson)

The stereocilia in a bundle are generally arranged in a hexagonal pattern, with the kinocilium at one end. Often, the bundle is approximately symmetric about a line running through the kinocilium. This horizontal line is usually called the line of bilateral symmetry. This line of symmetry is sometimes referred to as the E-I (Excitatory-Inhibitory Axis) because in many bundles, deflection along this axis in the direction of the kinocilium causes an excitatory response, while deflection in the opposite direction results in an inhibitory response. It is important to note that E-I axis is defined in terms of physiologic response, while the line of bilateral symmetry is anatomical. Lines of stereocilia running parallel to the line of symmetry are commonly called rows, although they are sometimes referred to as columns. Stereocilia along a line perpendicular to a row are usually similar in height, with heights decreasing as one moves along the row away from the kinocilium. Figure 1.2a shows an overhead schematic of a large hair cell bundle.

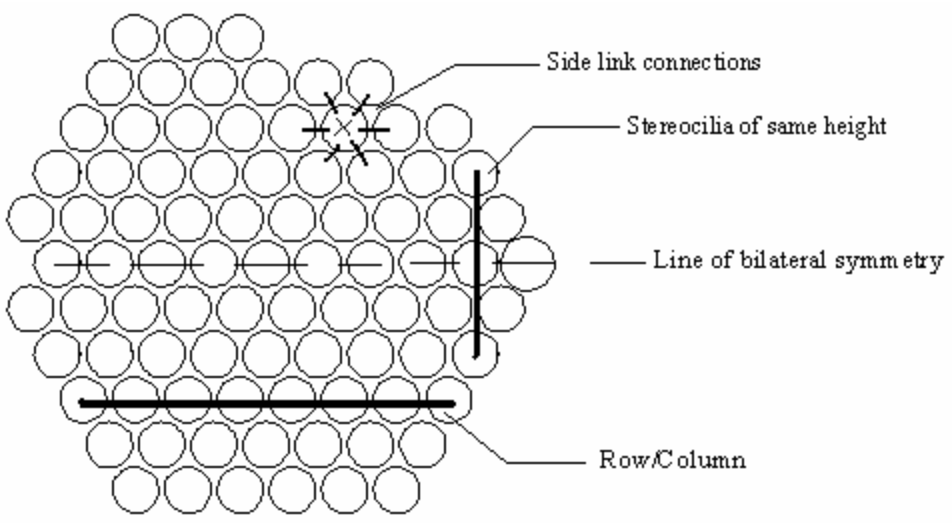

Figure 1.2a: Overhead schematic of a cell bundle

There are two types of hexagonal arrangements of cilia within a bundle, defined by Bagger-Sjoback and Takumida (1988) as loose packing and tight packing. Loose packing is the more common arrangement, in which rows of stereocilia run parallel to the axis of symmetry. The bundle in Figure 1.2a is loose-packed. In a tight-packed bundle, rows of stereocilia run at a roughly 30º angle to the line of bilateral symmetry, as shown in Figure 1.2b.

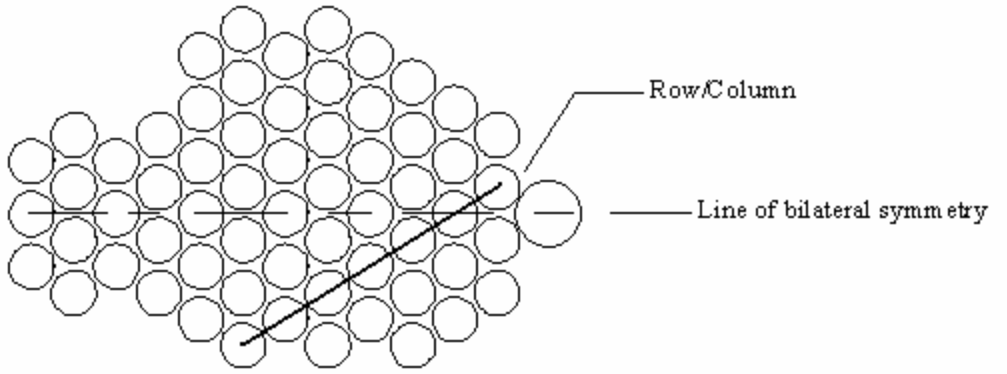

Figure 1.2b: Tight packed bundle schematic

Stereocilia are physically connected by many small fibers or links. Two types of links are found; tip links and side (or lateral) links. Tip links connect stereocilia in a row; so they run parallel to the line of symmetry in a loose bundle and at a 30º angle to it in a tight bundle. Each tip link runs from the tip of one stereocilium diagonally up to the side of the next tallest stereocilium in the row. Side links run parallel to the apical surface of the bundle and connect stereocilia to each of their nearest neighbors. There are several different types of side links: horizontal top links, found near the top of the cilia, shaft links, found lower down on the shaft of the cilia, and ankle links, found near the base of the cilia where the tapering occurs (Goodyear & Richardson, 1994). However, previous work (Cotton, 1998; Duncan, 1993) suggests that only the horizontal top links (often referred to as subapical bands) are structurally significant. Henceforth in this document, the terms "lateral links" and "side links" shall be used interchangeably to refer to the horizontal top links only. Refer back to Figure 1.8a for a visual illustration of this arrangement. Figure 1.3 shows a simple two-dimensional schematic of a bundle layout, including stereocilia, tip links, and lateral links, from a side view. This simplified schematic depicts a much smaller cell than that shown in Figure 1.2a.

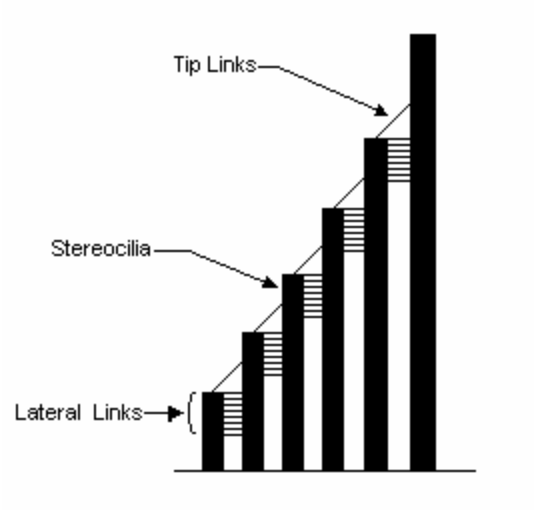

Figure 1.3: Bundle schematic, side view

The composition of the links is still unknown; their extremely small size makes them difficult to observe even with the aid of electron microscopy. Recent work (Kachar, et. al, 2000; Tsuprun, et al., 2002) has shown that tip links are right-handed, coiled

double or triple filaments that split at each end, forming two branches where the tip link contacts the taller stereocilium, and three or more branches at the tip of the shorter stereocilium. Materials that have been suggested for tip links and for side links include collagen, elastin, and the muscle protein titin. It is thought that tip and lateral links are composed of different materials.

Hair Cells: Physiology

Hair cells maintain a negative electric potential with respect to the surrounding endolymphatic fluid. When the stereocilia of the bundle are deflected by movement of the surrounding gel (or the cupula, inside the semicircular canals), ion gates located on the stereocilia open, allowing positive ions (potassium and calcium) to flow into the cell (Leish, et. al, 1999) via ion channels. The net result of the influx of ions is that the hair cell signals the neuron attached to it, and the information is carried to the nervous system. There are also believed to be mechanical effects on the bundle resulting from the opening of the ion gates; this possibility will be discussed later.

Directional Sensitivity

Hair cell bundles have been found to signal continuously (Shepherd & Corey, 1994, and many others), whether deformed or not, because even at rest, as many as 10% of the ion gates may be open (Kelly, 1991). Deformation of the bundle alters the signal by changing the number of open channels. Deflecting the bundle toward the kinocilium (the excitatory direction) increases the number of open ion channels, and the current flow increases (depolarization). Deflecting the bundle away from the kinocilium (the inhibitory direction), tends to decrease the number of open ion channels and reduces the current flow (hyper-polarization). Thus, hair cells exhibit directional sensitivity. A deflection perpendicular to the E-I axis has little to no effect on current flow (Lewis et al., 1985).

The orientation of hair cells in the vestibular organs allows the body to utilize their directional sensitivity. The hair cells are all oriented toward a curved path called the line of polarity reversal. Acceleration of the head, or a tilt of the head in a gravity field, in any direction, causes some hair cells to depolarize and others to hyperpolarize.

Depending on the pattern of hyper-polarization and depolarization, the brain can determine the direction of acceleration, or the orientation of the head.

Adaptation

Current flow is not constant under a static deflection. Experimental evidence (Eatock et al., 1987, Howard & Hudspeth, 1987, Shepherd & Corey, 1994, and others) has shown that the cell adapts to this deflection over a period of milliseconds. The current decays to approximately 20% of its original value (Leish, et. al, 1999). This adaptation allows the cell to be sensitive to small fluctuations around this new equilibrium point.

Experimental evidence has also shown that opening of ion gates correlates to a decrease in bundle stiffness. Howard and Hudspeth found in some bullfrog hair cells that as much as a 40% drop in stiffness resulted from approximately half the maximum number of channels being open (Howard & Hudspeth, 1987).

Three important questions arise. First, how does mechanical stimulation of the bundle cause the opening of ion channels? Second, how does the opening of ion gates result in increased bundle compliance (decreased stiffness)? Third, how does the bundle adapt to a static deflection?

It is currently believed, though not proven, that deflection of the stereocilia "tenses elastic elements" (Howard & Hudspeth, 1988) known as "gating springs" that pull directly on the channels. Increasing tension in a gating spring increases the probability that the channel it is connected to will open. Perhaps the tension influences a protein that can change configuration; in one configuration, it blocks the channel; in the other, the channel is open. Most researchers in the field currently believe that tip links control the channels, either by acting as the gating spring element or by being in series with the spring. If this theory is correct, tip link tension (influenced by stereocilia deflection) is the key factor in controlling whether ion gates are open or closed.

One theory as to how opening of ion gates decreases bundle stiffness is quite simple. According to the theory, when an ion gate opens, it decreases the amount that the gating spring is stretched, reducing the tension in the spring (Howard & Hudspeth, 1988). The other theory involves molecular motors.

Molecular motors are a possible answer to both the bundle adaptation question, and the connection between ion gates and increased bundle compliance. It is hypothesized that the upper end of each tip link is connected to a molecular motor that is constantly exerting an upward force on the tip link, trying to pull it up the taller stereocilia. This action ensures that the tip links are always kept in a state of tension, and would account for ion gates being open even when the bundle is at rest: some of the tip links are under sufficient tension to open their gates. This phenomenon is often referred to as "pre-tensioning." When the bundle is deflected, tip link tensions rise, and cause more ion channels to open. The influx of calcium and potassium ions somehow causes the molecular motor complex to slip and by "slackening the link's tension" (Leish, et. al, 1999), allows the ion gate to close under constant deflection. Once the gate shuts, the calcium and potassium influx stops, and the motor can resume its climb, restoring the resting tension level. Some experimental evidence for the molecular motors exists. Electron-dense "plaques," (Holt & Corey, 2000) located on the stereocilia near the point of tip link attachment, are believed to be the molecular motor complexes. Experiments in which tip links were cut with the compound BAPTA showed that these plaques moved upward 50-70 nm, as one would expect the molecular motors to do if they were suddenly unrestrained (Holt & Corey, 2000). Recent work has obtained substantial evidence that myocsin-1c is the hair cell's molecular motor (Holt, et al., 2002).

Another hypothesis described by Holt & Corey (2000), involves calcium ions bonding to sites near the channels and altering the probability response of the gates, such that higher tension levels would be required to maintain an open configuration. This change would tend to close channels unless higher tension levels were reached, creating a new resting point at the static deflection.

Other theories

One other theory of note is that electrostatic interaction between stereocilia may play a role in the mechanical behavior of the bundle (Dolgobrodov, et. al, 2000; Neugebauer & Thurm, 1987). Stereocilia are believed to possess an extended, negatively charged surface coat, known as a glycocalyx. Interactions between glycocalices of neighboring stereocilia could cause the stereocilia to attract or repel each other.

Experimental evidence for the theory does exist; researchers have shown that spatial separation between stereocilia could be altered by changing the ionic composition of the solution that the hair cell was in (Dolgobrodov et al., 2000). However, a major limitation of the theory is that electrostatic interaction is only significant over a very short distance, on the order of 0.8 nm or less (Dolgobrodov et al., 2000).

Mechanical testing of bundles

Many experimenters (Crawford & Fettiplace, 1985; Howard & Hudspeth, 1988, Howard & Ashmore, 1986, and others) measure the stiffness of hair cell bundles by stimulating them with a quartz or glass probe that is "mechanically coupled to the rows of the tallest stereocilia in the bundle" (reviewed in Szymko, et. al, 1992). Through knowledge of the probe stiffness and deflection, one could determine the force on, and displacement of, the bundle. One group of researchers (Szymko, et. al, 1992) used a water jet rather than a mechanical probe to deflect bundles. Researchers often simultaneously measure hair cell current using microelectrodes.

Motivation for Modeling

Hair cell bundles occur in many shapes, sizes, and arrangements in the body. The heights, positions, and numbers of stereocilia vary widely from cell to cell. Presumably, these morphological variations serve a practical purpose. But what purpose? Ultimately, a successful model could help researchers understand the effects that these variations have on the mechanical response and behavior of the bundles.

Why not simply use experimental methods? Due to the extremely small nature of hair cells, and the often dense arrangement of them, it is difficult and time-consuming to stimulate a single specific bundle accurately. A sufficiently accurate model could in theory give you essentially the same results from just the structural data (stereocilia heights, positions, etc). While obtaining accurate structural data is not easy either, it is probably less daunting than making accurate measurements on live bundles. By taking measurements from various regions of the vestibular organs, and obtaining model results for these cells, one could begin to correlate cell location with function.

Also, as was mentioned earlier, questions about both anatomy (link composition) and physiology (adaptation, molecular motors, etc) still persist. By mechanically modeling theories that explain unanswered questions, the feasibility of those theories can be tested. For example, one could change the tip link properties in the model to match those of a material hypothesized to compose the tip links, and see if the model's results are realistic or not. Many of these properties currently cannot be measured directly; modeling is the only method to determine them.

Previous Research Work and Modeling Assumptions

Many researchers, such as Pickles (1993), used a simple lumped parameter model, in which stereocilia are rigid shafts attached by torsional springs at the cuticular plate, with springs for the tip and lateral links. Later models (Shepherd & Corey, 1994, Howard & Hudspeth, 1987, and others) included additional terms, such as viscous damping.

The first finite element model was created by Duncan & Grant (1997), using commercial finite element software. It was limited to a single column of stereocilia, but provided useful results. A significant discovery from this model was stereocilia must be modeled anisotropically for realistic results. Attempts to model stereocilia isotropically resulted in either buckling of the bundle, or bundle stiffness values well below those observed experimentally.

Cotton (1998) continued work in the area by creating a custom Fortran code that incorporated anisotropic stereocilia, and allowed modeling of fully three-dimensional bundles. Most researchers (Shepherd & Corey, 1994, Howard & Hudspeth, 1987, etc) use some variant of Pickles' lumped parameter model and restrict their work to two dimensions, which makes Cotton's work unique. Cotton modeled the body of the stereocilia using Timoshenko (shear deformable theory). Unlike classical Euler beam theory, Timoshenko theory allows deflection and rotation of elements to be independent degrees of freedom. Figure 1.4 illustrates a Timoshenko beam element before and after deformation. Deflection and rotation are represented by "w" and "ϕ" respectively.

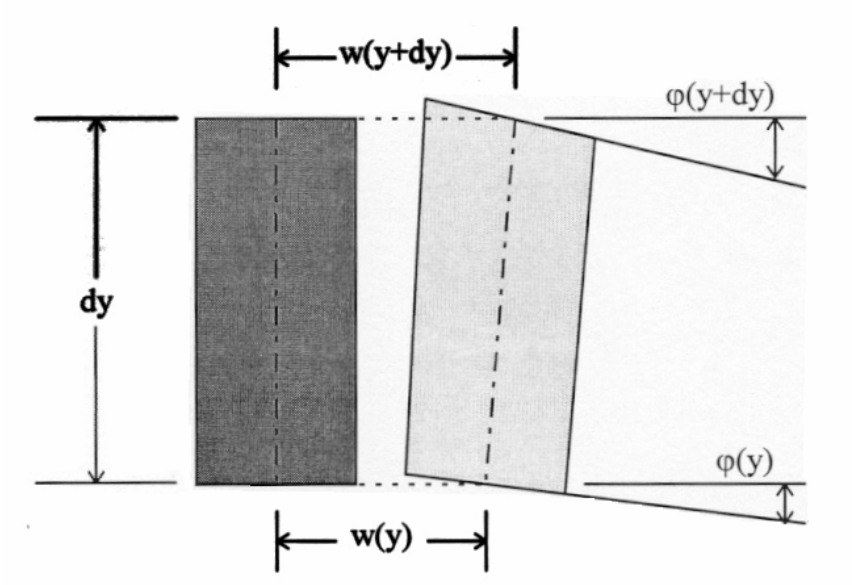

Figure 1.4: Timoshenko beam element, before and after deformation (Cotton, 1998)

Summary of thesis research

Continuing Cotton's work, I used his model to examine several 3-D bundles modeled after real bundles from various locations in the utricle of the red-eared slider turtle. I created and examined stiffness curves and patterns of tip link tensions to further explore aspects of three-dimensional bundle mechanics, as there is no other published work in that area. Although these experiments were not originally intended to be the primary focus of this thesis, so many intriguing results relating geometric and material properties to bundle response were obtained that this section developed prime importance.

While Cotton's model produced useful results, it did not incorporate some of the more complicated aspects of bundle behavior, such as ion gates/channels controlled by tip link tension, molecular motors, pre-tensioning, adaptation, and ion channel-induced bundle compliance. An important goal of this thesis was to investigate some of these more complicated aspects of bundle behavior and attempt to improve Cotton's program by incorporating them into it. By evaluating the results of implementation of these concepts in the model, I hoped to gain a more complete picture of how real bundles might operate mechanically, and what assumptions about bundles are realistic.

A third goal was to determine if we could establish a better estimate of the tip link elastic modulus, based on the response of the bundle to loading for various values of the tip link modulus.

Organization of the thesis

Having given some basic background information on hair cells and the vestibular system, as well as the current state of knowledge in the field, I will next explain the workings of Dr. Cotton's program in more detail in Chapter 2. Chapter 2 also describes further the methods used for my research. After that, I will detail the results I obtained and discuss their implications, dividing the subject into two chapters: Chapter 3 covers the basic investigations that utilized Cotton's program without modifications; Chapter 4 describes the work done on implementing ion gates and other complex features, and the results obtained. Chapter 5 summarizes the key results and comes to some overall conclusions, and suggests future directions the research should explore.

CHAPTER 2: METHODS AND MATERIALS

Most mathematical modeling of hair cell bundles currently in the literature (for example, Jacobs & Hudspeth, 1990; Pickles, 1993; Duncan & Grant, 1997, and others), model bundles with the stereocilia in a single row. Further, many of these models are so-called "lumped parameter", in which cilia are represented by rigid beams connected to each other by linear springs, with torsional springs at the base (for example, Pickles, 1993).

Cotton, as mentioned in Chapter 1, created a Fortran code that allows three-dimensional finite element modeling, which I used (with some modifications) for the research presented in this thesis. For full details on Cotton's program, readers are referred to his dissertation (Cotton, 1998); however, I will summarize many of the key features of the program in this chapter. I will also discuss limitations of Cotton's code/modeling method, detail how the model was utilized in this research, and discuss some of the modifications that I made to the program. Later in the chapter, I discuss the specific hair cell bundles that I studied, and how data for them was obtained.

Model Features

As explained in the introduction, Cotton's code (henceforth referred to by the program's name, "*bmod*", which stands for bundle modeler), models the cilia as Timoshenko beams. Since *bmod* uses finite element techniques, each cilium is divided up into elements. Each element is bounded by two nodes, one at the top and one at the bottom. Each node has five degrees of freedom: x, y, and z displacement, and 2 degrees of rotation (rotation about the long axis of the cilia is not permitted). The differential equations used in Timoshenko theory, as well the derivations and explanations of the stiffness matrix, equation assembly, and other technical details of the finite element process can be found in Cotton, 1998, and in Cotton and Grant, 2000.

Recall that cilia are connected by two types of links: tip and lateral. These links are modeled as two-force members connecting two cilia together, and exhibit linear spring behavior (although the linear aspect can be modified, as I explain later in this chapter). In *bmod*, lateral links are not allowed to carry compressive loads; they buckle

and are removed from the model if they go into compression. This behavior occurs frequently. Tip links do not generally go into compression, and *bmod* does not account for their buckling; however, I made a related modification to the program for some of my research that deals with situations where tip links go slack; see the Modifications section for details.

In addition to connecting cilia to each other, *bmod* specifically deals with their attachment to the underlying cuticular plate. Either pinned or cantilevered boundary conditions can be imposed. In actual cells, stereocilia are cantilevered because actin filaments extend into the cuticular plate, while kinocilia are free to pivot at the base. This approach was verified by Duncan, 1993.

Bmod allows external point forces to be placed on a cilium (or cilia); conventionally it is applied to the kinocilium. Rather than calculating the deformation of the bundle under a given load directly, *bmod* ramps up the force gradually (in user-defined increments), calculating the intermediate deformation at each step. The intermediate deformation affects calculation of the stiffness matrix for the next step, and so on. This method is often referred to as "load following". Load following is one aspect of geometric nonlinearity that *bmod* employs. Further accuracy is obtained through a technique called "booming" (Cotton, 1998). Succinctly put, booming means correcting the orientation of links (or rather, the forces exerted by links) to take into account deformed geometry. Figure 2.1 shows the effects of booming. Part A shows the un-deformed geometry. Part B shows the deformed geometry without booming; note that the link runs directly between the centers of the two cilia. The link's orientation is unaffected by the rotation of the cilia. Part C shows the deformed geometry with booming correction; the link runs edge-to-edge, and its orientation is correctly affected by the rotation of the cilia. Note that in addition to corrections needed for horizontal displacements as shown, corrections needed for vertical movement (due to bending of the cilia, for instance) are also needed.

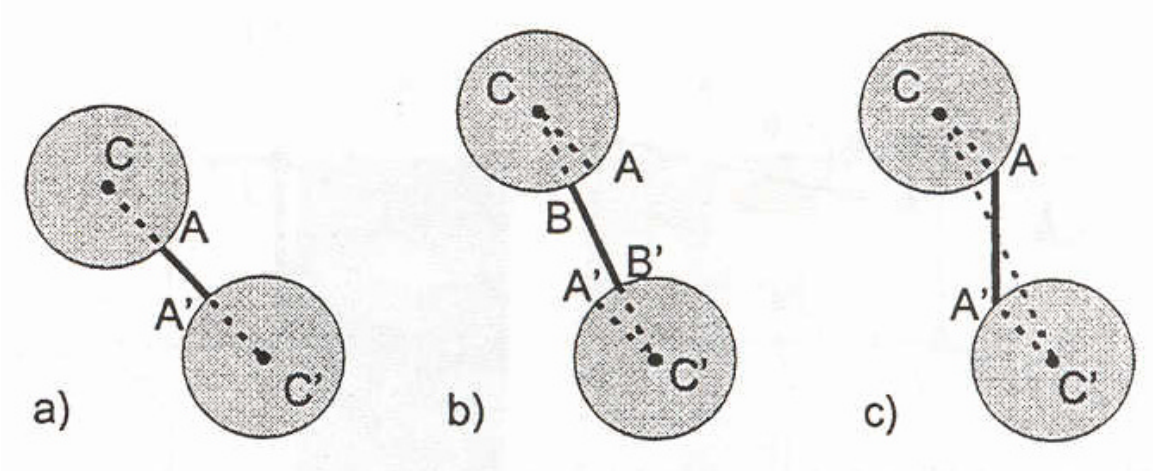

Figure 2.1: Booming correction illustration (Cotton & Grant, 2000).

At each force step, *bmod* iterates, recalculating the stiffness matrix and obtaining new deformations. Buckled links are removed, booming corrections are made, and convergence must occur before the program moves to the next step.

Bmod allows the user to specify the geometric layout and properties of the bundle, the force-loading scheme, and the material properties, via an input file. Cilia locations, heights, and diameters, link locations and diameters, and material properties of both links and cilia are specified. In addition, the applied loads, force-step increments, and element sizes are enumerated.

Model Limitations

Two primary limitations of *bmod* exist. First, the program models bundles as static, when in real life, bundles are dynamic systems. Although the force and deflection on the bundle are calculated iteratively, no representation of time passage occurs; *bmod* models an instantaneous response. No mass matrix or inertial terms are calculated in the finite element process. Consequently, adaptation behavior cannot be modeled. Molecular motors cannot re-tense tip links. In order to fully model a bundle, time must be allowed to elapse; however, much can be learned about bundle mechanics from a static model. The only dynamic aspect of bundle response investigated in this thesis involves modeling ion gates; see Modifications for more details.

The other primary limitation of *bmod* is not due to the program itself, but would affect any mathematical model of bundles: property uncertainties. Cilia are known to be composed of actin filaments, but the composition of tip links and lateral links are unknown, and it is believed that the two types of links are composed of different materials. Material properties are extremely difficult to measure in such small biologic components. Geometric properties are also difficult to determine accurately. Uncertainties in the input to the program are a limitation on the accuracy of the program's output, no matter how realistically the equations are used. In the "Cells Modeled" section of this chapter, I describe how these properties were obtained or estimated for this research. In part of Chapter 3, I discuss the effects of varying some of these properties.

Modifications

The two primary modifications that I made to the *bmod* program were the implementation of tip link slackening and ion channels. Tip link slackening worked in much the same way as lateral link buckling: if the two nodes that marked the ends of the tip link moved closer together than their initial spacing, the tip link would effectively go into compression, and be removed from the model. The only difference was that tip links were allowed to re-tense if conditions were appropriate, such that if the link was re-added to the model, it would be in tension again; lateral links were removed permanently if they buckled.

The second modification was implementation of ion channels. The opening of a channel was controlled by the tension in its tip link; once the tension reached a specified threshold, the gate opened and remained "locked open" for the duration of the run. The mechanical effect of an opened gate was an increase in the length of a tip link; this increase causes the tip link to decrease in tension (or even go slack), causing a drop in bundle stiffness.

Two other features were tested: pre-tensioning of tip links, and variable tip link elastic modulus. Pre-tensioning refers to a pre-existing tension in tip links when the bundle is not loaded; by variable tip link modulus, I mean the elastic modulus varies depending on strain in the tip link (strain-hardening behavior, in this case). The version

of the *bmod* program with these features was NOT used for the work shown in Chapter 3, and was only used for the work described in Chapter 4.

Cells Modeled

Models of six real hair cell bundles from the utricle of the Red Eared Slider Turtle (*Trachemys* (*Pseudemys*) *scripta*) were used in this research. The obtaining of the data for these models, and the translation of the data into viable input files for *bmod*, was completed as part of the research work done by Grant, Cotton, and Peterson during the late 1990's (Cotton, et al., 1998). I am explaining the process because it adds validity to the modeling work to show the biological basis. Juvenile turtles that had similar ages and carapace lengths (ranging from 8 to 11 cm) were used as sources of turtle utricles. Each turtle was euthanized with an overdose of sodium pentobarbital. The inner ear was removed, and placed in pH adjusted custom formulated turtle Ringer's solution. All animal care protocols and guidelines were followed. The utricle was then dissected and further processed for SEM and light microscope study (Silber, Cotton, Peterson, Grant, manuscript in preparation).

These six bundles were chosen because they illustrate the variation in bundle structure and fundamental bundle types seen throughout the utricle neuroepithelium of this turtle species. The bundles were taken from a transect (a long rectangular area of finite width) running from the nerve entrance (medial) across the utricular neuroepithelium to the area where the two semicircular canal ampula are located (lateral). This transect is again representative of the hair cell bundles of the whole utricle. The six bundles are numbered in order of their position along the transect from medial to lateral (Silber, Cotton, Peterson, Grant, manuscript in preparation). All six bundles are thought, with some certainty, to belong to Type II cells (Peterson, 2002).

Figure 2.2 shows the six bundles chosen for research. In this figure both an SEM photomicrograph and a computer generated 3-D rendering for each bundle are presented. The SEM's are of bundles that were subjected to ultrasound, breaking off the stereocilia; what remains are the stumps of each individual stereocilium. This surface SEM was used to obtain the geometric distribution of the stereocilia in the plane of the neuroepithelium (Peterson, et al., 1996). SEM photomicrographs of whole bundles, along with DIC light

microscope observations of live bundles, and studies of kinocilium height (Fontilla and Peterson, 2000), were used to define heights of stereocilia and the kinocilium. The height data was obtained from various bundles that were different from, but similar to, the original bundle. In this manner a realistic representation of a bundle was assembled. The computer-generated graphic for each bundle in Figure 2.2 is based on the model input into *bmod*, and shows the deformed state of the bundle. Although it may not be clear from Figure 2.2, cells 1, 2, 4, and 5 are "loose-packed", and cells 3 and 6 are "tight-packed", as defined in Chapter 1.

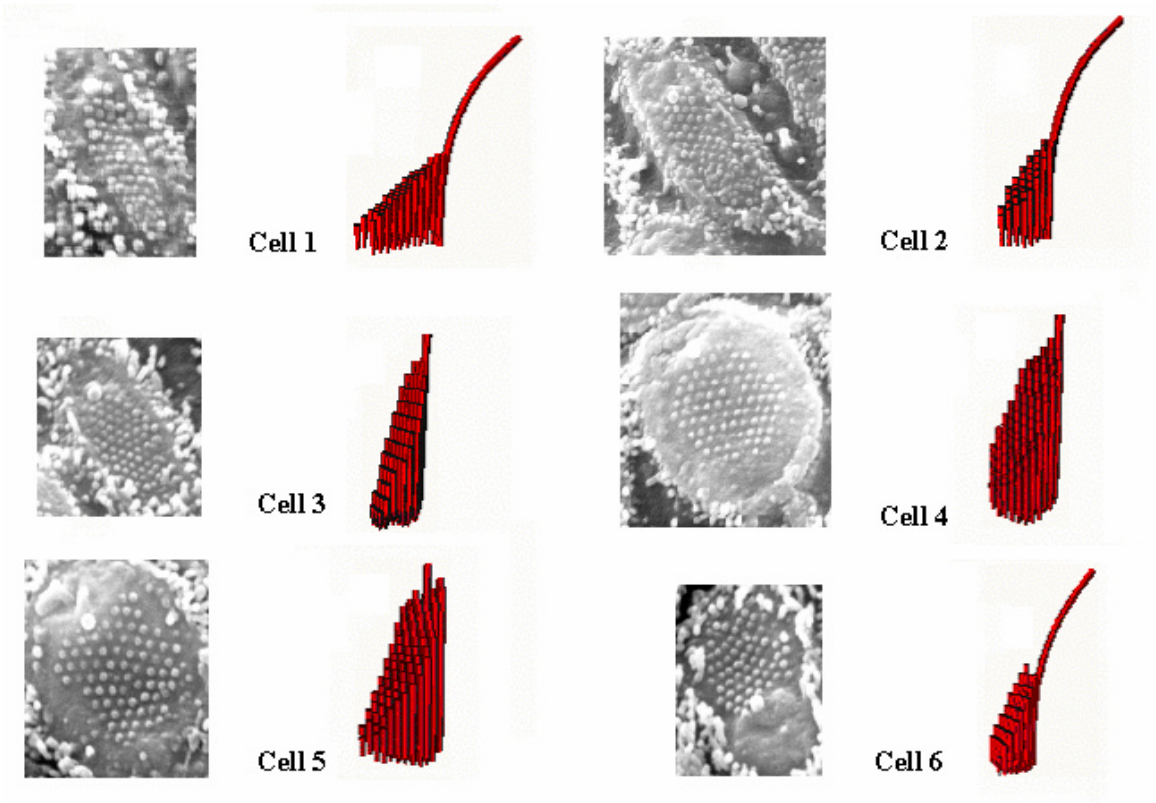

Figure 2.2: Six utricle cells – electron micrograph and 3-D rendering

Obviously, many approximations were made in modeling the cell bundles. Stereocilia diameters and spacing were approximated as constant throughout a given bundle. Perfect hexagonal layouts do not exist in biological bundles, but they are much easier to model. Cilia heights were based on similar bundles, and were approximated so as to linearly decrease in height along the E-I axis. Tapering at the base of stereocilia was

approximated based on visual examinations of living bundles. Locations of tip and lateral links had to be guessed at based on other research due to their extremely small size. Link diameters used values obtained from published sources.

Initial testing revealed a non-biological bundle stiffness "dip" at low deflections, which was caused by lateral link buckling. This reduction is stiffness is not seen in any experimental measurements or bundle modeling, other than this three-dimensional model, and for those two reasons we deemed this type of behavior to non-biological. It indeed may be realistic, however, the collective wisdom is that it is not biologic. In order to correct this, I removed certain key lateral links that were buckling, generally 5 to 10 sets. There was no particular pattern to which links buckled, except that none of the links were parallel to the axis of symmetry. The specific links were determined by trial and error for each cell bundle. I acknowledge that this is a future issue that needs to be solved, but for the purposes of this research, the aforementioned solution was implemented.

Tables 2.1 through 2.4 list some the properties used in modeling the six cells. Table 2.1 lists the geometric parameters common to all six cells, while Table 2.2 lists the common material properties. Note that some of these properties (namely, tip link elastic modulus) are varied in some of the studies mentioned later on in this thesis; these variations are made clear when they occur. Table 2.3 and 2.4 list specific geometric parameters by cell: Table 2.3 lists cilia spacing, counts of links, cilia, and rows, while Table 2.4 lists specific cilia geometric properties such as diameter and height (Silber, Cotton, Peterson, and Grant, manuscript in preparation). When possible, the source or reference used to determine the value is given. Explanatory notes follow each table, as needed. These abbreviations are used: ster = stereocilia; kino = kinocilium.

Table 2.1: Common Geometric Properties

Property	Value	Source/Reference
Kinocilium diameter	0.35 µm	Measured
Stereocilia taper height	1.0 µm	Measured
Tip link diameter	10 nm	Kachar et al., 2000 Tsuprun & Santi, 2000
Lateral link diameter	9 nm	Cotton, 1998 Duncan & Grant, 1998 Duncan, 1993

Notes: Stereocilia taper height refers to the vertical distance along the stereocilia during which tapering from the full diameter to the diameter at the base of the stereocilia occurs.

Table 2.2: Cell Bundle Geometric Properties

Cell	Array Type	# of Cilia	# of Rows	# of Tip Links	Stereocilia Spacing, µm	# of Lateral Link Sets
1	Loose	50	5	44	0.280	108
2	Loose	35	6	28	0.280	80
3	Tight	62	9	51	0.280	141
4	Loose	86	11	74	0.340	220
5	Loose	78	11	66	0.340	186
6	Tight	54	9	44	0.280	122

Notes: Array type refers to the tight packing or loose packing, as defined by Bagger-Sjoback and Takumida (1988) and explained in Chapter 1. Stereocilia spacing is center to center, in any direction in which lateral links connect (see Figure 1.8a in Chapter 1). A lateral link set is all the lateral links connecting any 2 given stereocilia.

Table 2.3: Cilia Geometric Properties

Cell	Ster. Diam, µm	Ster. Diam at base, µm	Ster. Height Range, µm	Kino. Height, µm
1	0.24	0.04	1.2 – 3.9	14
2	0.24	0.04	1.3 – 3.8	14
3	0.24	0.04	1.2 – 7.8	9
4	0.30	0.05	1.6 – 8.0	9
5	0.30	0.05	1.1 – 8.2	9
6	0.24	0.04	1.1 – 5.5	14

Notes: Stereocilia height range refers to the heights of the shortest and tallest stereocilia in the bundle; generally the tallest stereocilia are closest to the kinocilium and the shortest are in the periphery of the bundle.

Table 2.4: Material Properties

Material Property	Value, N/m^2	Source/Reference
Kinocilium Young's modulus - E_k	1.3×10^8	Cotton, 1998
Kinocilium shear modulus - G_k	4.6×10^7	Adjusted to be isotropic; Cotton, 1998
Stereocilia Young's modulus - E_s	3.0×10^9	Gittes et al., 1993
Stereocilia shear modulus - G_s	1.43×10^6	Cotton & Grant, 2000 Cotton, 1998
Tip link Young's modulus - E_{TL}	1.0×10^7	Chosen to be within reasonable range of values

CHAPTER 3: THREE-DIMENSIONAL BUNDLE MECHANICS

As explained in Chapter 2, six cell bundles were used for this series of experiments. The overall goal was to better understand bundle mechanics, and in particular, the effects of bundle geometry and material properties on the mechanical response of true three-dimensional bundles.

Procedure

Details and specifications on the six sample cell bundles used can be found in Chapter 2. Unless otherwise noted, cells were loaded by a point force applied at the tip of the kinocilium, acting along the line of bilateral symmetry, in the excitatory direction. Recall that in the case of loose-packed cells (1, 2, 4, and 5), the rows run parallel to the line of symmetry. In tight-packed cells (3 and 6), the rows run at a roughly 30º angle to the line of symmetry. The applied load was increased gradually from 1 pN up to 500 pN, and the resulting displacements, stiffness, and tip link tensions were determined.

Tip Link Tensions and Bundle Stiffness

Results

The tip link tensions for each cell are shown in Figure 3.1. The tensions shown occurred under an applied load of 200 pN. Each circle in the figure represents a cilium, and each line connecting cilia represents a tip link. The number inside each circle is the tension (in pN) of the tip link connecting that cilium to the cilium on its right (i.e. the next taller cilium). K represents the kinocilium, N means there is no tip link running to the right of that cilium, and S means a tip link is slack. The shading in the circle relates that tension value to the other values in the bundle. The darker the shading, the higher the relative value, so pure black represents the highest tension.

I will discuss tip link tension distributions later in this chapter, but for now, note that the tensions vary significantly within each bundle, with the highest tensions (darkest circles) found near the kinocilium. Also note that the maximum tension varies between

bundles; cells 1, 2, and 6 have maximum tensions of 100 pN or higher, while cells 3, 4, and 5 have maximum tensions of less than 40 pN.

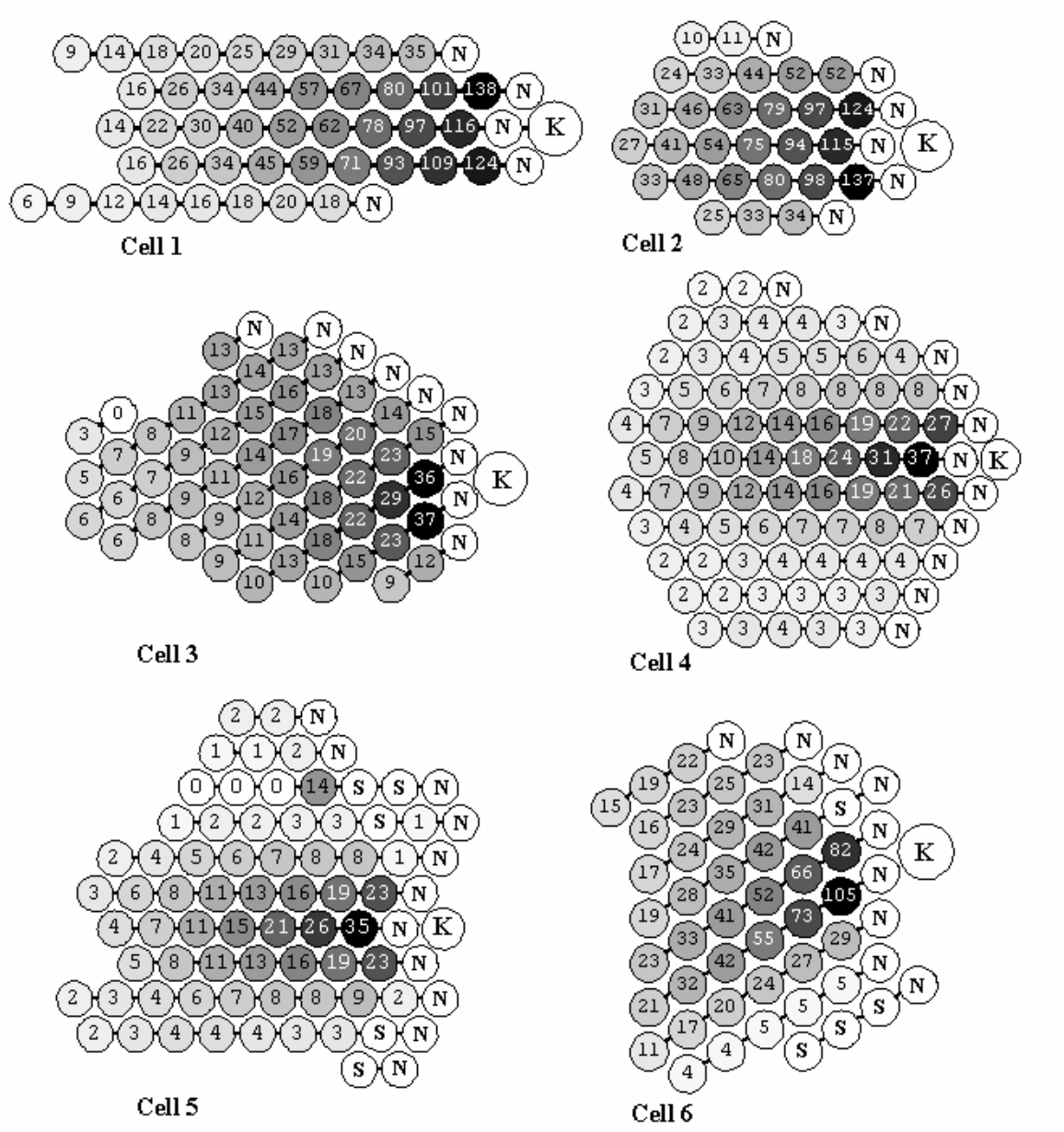

Figure 3.1: Tip link tension distribution under a 200 pN applied load

Figure 3.2 shows information about the bundles' stiffness. Part I of the figure shows the bundle stiffnesses under a 500 pN applied load. Note that the stiffnesses of cells 3, 4, and 5 are an order of magnitude higher than those of cells 1, 2, and 6. The

bundles can thus logically be grouped into two sets: a Stiff group (S Group) and a Compliant group (C Group). Part II shows the stiffness vs. deflection plot for each bundle, with the stiffness for each bundle normalized by that bundle's initial stiffness (approximated by the stiffness at a 1 pN load). Note that C Group and S Group exhibit different behaviors: C Group stiffnesses "level off" at low applied loads, and do not reach the higher values that S Group bundles do. Part III and Part IV show the absolute stiffness vs. deflection for the two groups; note the difference in scale.

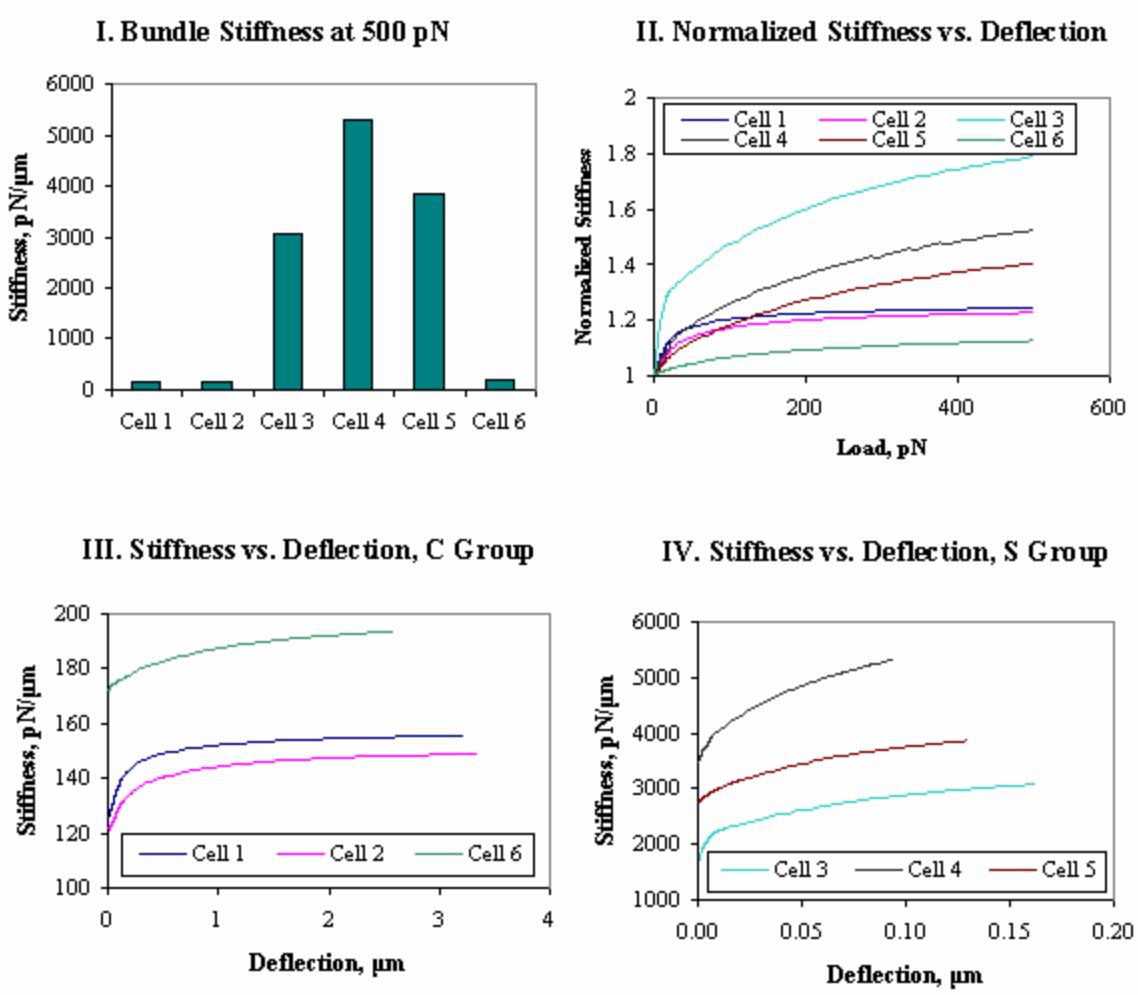

Figure 3.2: Stiffness results

Now that the distinctions between C Group and S Group are evident, revisit Figure 3.1 and compare the tip link tension plots again, looking at the highest tension in

each bundle. C Group (cells 1, 2, and 6) has maximum tip link tensions of more than 100 pN; about 3 times as high as the highest tensions in S Group (cells 3, 4, and 5).

In summary, three key differences in mechanical response are evident between the two groups: an order of magnitude difference in stiffness at a given load, the amount of "growth" of stiffness as deflection increases, and the magnitude of maximum tip link tensions at a given applied load. Since identical material properties are used for each cell, and identical loads were applied to each cell, the differences must be due to morphology: the arrangement of links and the number, heights, and arrangement of cilia.

Discussion

Two easily quantifiable morphological differences help distinguish the two groups. First, the number of cilia per bundle is greater in S Group than in C Group. Second, the height ratio of the tallest stereocilia to the kinocilium is also higher in S Group than in C Group. The numerical details are given in Table 3.1 (organized by Group).

Table 3.1: Morphological differences

Group	Cell	# of Cilia	Height Ratio
C	1	50	0.279
C	2	35	0.271
C	6	54	0.393
S	3	62	0.867
S	4	86	0.889
S	5	78	0.911

Figures 3.3a, 3.3b, and 3.3c shows the results of attempting to quantify the relationship between each of the two morphological differences and each of the three mechanical or behavioral differences mentioned previously, by measuring the R^2 value of a fitted line. An R^2 value close to 1 suggests a strong relationship, while an R^2 value close to 0 suggests no relationship. Although the small sample size (N=6) limits the significance of the analysis, the results are worth considering. This analysis was

suggested by Dr. John Cotton, and utilizes unpublished work of his (Silber, Cotton, Peterson, Grant, manuscript in progress).

Figure 3.3a shows plots of stiffness against # of cilia and height ratio. Cell numbers are printed next to their respective data points. Intuitively, one would expect that more cilia would result in a stiffer bundle, as there would be more resistance to deformation, and the R^2 value of 0.89 supports a strong correlation. However, the correlation between stiffness and a large height ratio is nearly as high (0.86). This correlation suggests that taller stereocilia are more effective in supporting a bundle than shorter ones. One possible explanation for this difference is that because taller stereocilia attach to the kinocilium at higher points, less of the kinocilium is free to bend. Since the kinocilium is essentially acting like a beam, the shorter the effective length, the more force it takes to deflect it, and the stiffer it will seem.

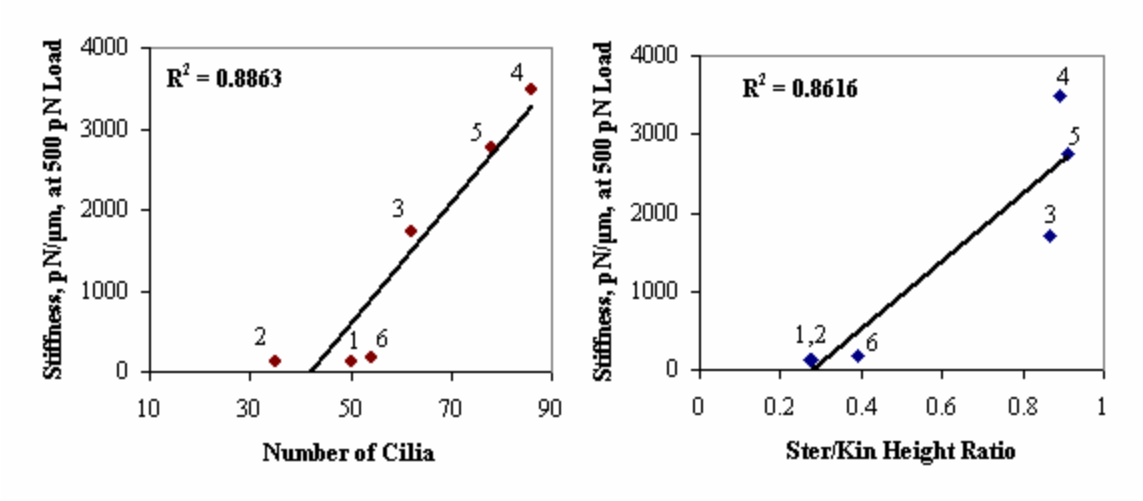

Figure 3.3a: Correlation between morphology and bundle stiffness

The second pair of graphs, Figure 3.3b, involves the percent change in stiffness from the initial stiffness (1 pN load) up to the stiffness under a 500 pN load. Here, the number of cilia correlates poorly. The height ratio correlates moderately well, with an R^2 of 0.62.

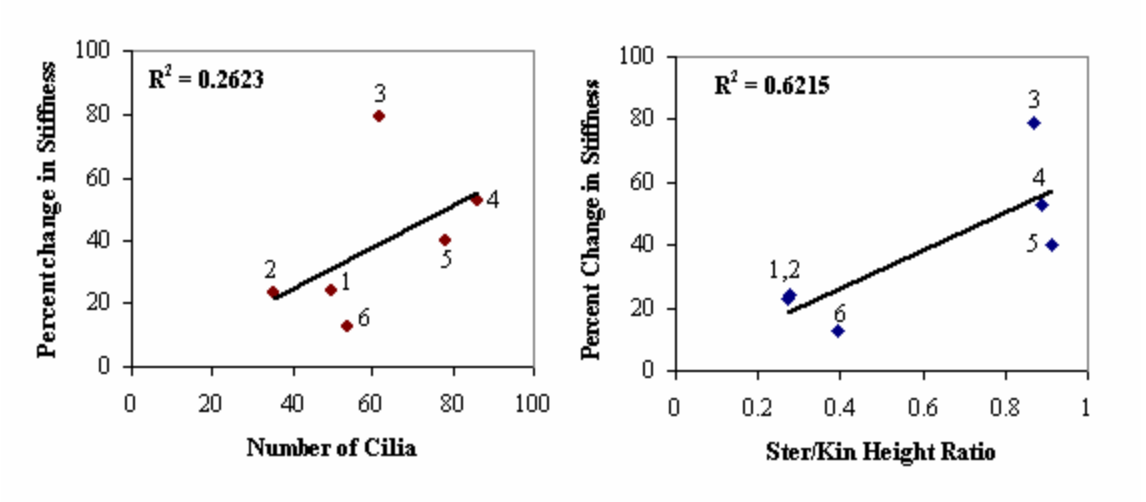

Figure 3.3b: Correlation between morphology and percent change in stiffness

A probable explanation for why there is any significant increase in stiffness at all is "recruitment". By recruitment, I mean that as the kinocilium deforms further and further, the links connecting it to neighboring stereocilia are stretched, and these nearby cilia are "recruited" (i.e. pulled in) to help resist the applied load. As more and more stereocilia are recruited, the overall bundle stiffness increases. Another way to think of recruitment is in terms of link reorientation. Recruitment causes the force vector of links in adjacent rows to turn inward so as to oppose further bundle deflection.

It should be noted that experimentally, some researchers have found bundle stiffness to be relatively constant with deflection (Howard & Ashmore, 1986, for instance), while relatively few (Silverman, 2002, for instance) have found bundle stiffness to increase with deflection. Several possible explanations exist for this discrepancy. Many of the constant stiffness results came from bullfrog hair cell bundles, which are geometrically different from turtle cell bundles. In bullfrog cell bundles, the cilia are aimed toward the bundle center, making the bundle resemble a cone, while in turtle cell bundles, the cilia are more or less vertical. The orientation of cilia in bullfrog cells may prevent "recruitment" from occurring, and thus keeping the stiffness constant. Another possible explanation is that in real cells the stiffness increases occur over relatively small deflections and then level out (like the "C group" cells did here).

Experimental techniques may not be precise enough to test stiffnesses at small enough deflections to detect the increase. A third possibility is that the wide spread in most of the stiffness data collected is masking an increasing stiffness trend.

The causes of the relative amount of stiffness increase are not as clear. One might expect a strong correlation with the number of cilia, as more cilia could be recruited, and resist the deformation. From Figure 3.3b, the correlation is very weak. However, if one looks at Figure 3.2, Parts III and IV, one notices that in the C Group cells (especially 1 and 2), stiffness "growth" occurs mainly at low applied force values, and levels off quickly. If one were to continue increasing the load beyond 500 pN, the stiffness would most likely not increase significantly. In contrast, in S Group, the stiffness growth shows no evidence of leveling out, and would most likely continue to grow.

Another factor to consider is that the positions of the stereocilia may be just as important as the number of them. With this idea in mind, note that in Figure 3.3b, the left graph has 2 apparent outliers (cell 6 and cell 3); as it turns out, these two outliers are both tight-packed bundles. It is possible that the unusual structure of the tight-packed bundles is another key factor. If these two outliers are removed, the best-fit line has an R2 value of about 0.9. The statistical significance of this value is doubtful due to the small sample size; however, it is an interesting side note.

Finally, we examine the maximum tip link tension (in each bundle) and normalize it according to the applied load (200 pN). These results are plotted in Figure 3.3c. The R^2 value when this is plotted against the number of cilia is decent (0.77), but an amazingly high R^2 value of 0.99 results when it is plotted against the stereocilia/kinocilium height ratio. This unusually high value is achieved because the all the cells (except cell 6) are clustered into 2 groups: the C Group cells (except cell 6, which is nearby) are clustered together, and the S Group cells are clustered together.

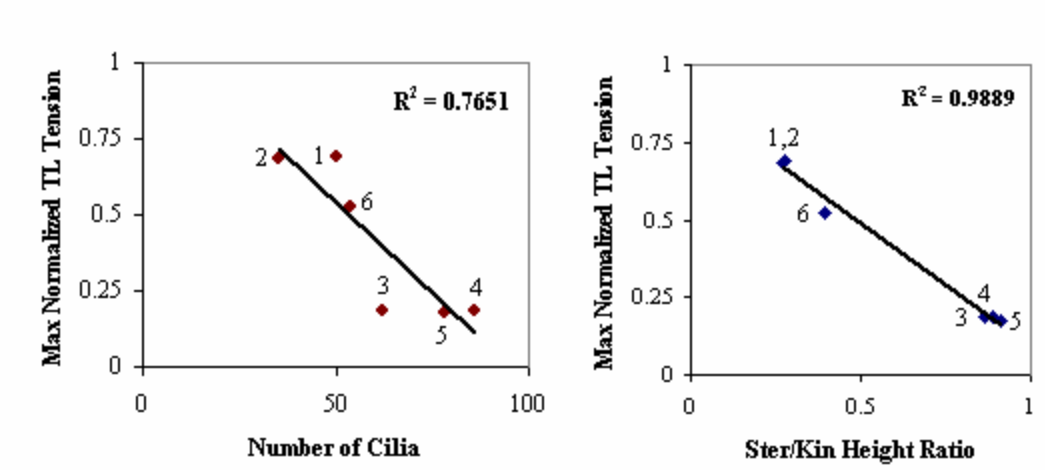

Figure 3.3c: Correlation between morphology and maximum normalized tip link tension

In general, these results seem to suggest that the stereocilia/kinocilium height ratio is the most significant morphological factor in influencing these aspects of bundle mechanics. As a quick experiment, I modified cell 1's height ratio to match the S Group ratios, simply by increasing the stereocilia heights (no other changes were made). As a result, bundle stiffness at 500 pN load increased by an order of magnitude from 125 pN/μm to 1086 pN/μm. Maximum normalized tip link tension increased from 0.3 to 0.7. The percent increase in stiffness increased from 24% to 36%. In summary, all three behaviors changed to become very similar to S Group, helping confirm the importance of the stereocilia/kinocilium height ratio.

Effect of Cilia Diameters

One final morphology difference can be brought up: the two stiffest cells, cell 4 and cell 5, have larger cilia diameters than the other 4 cells (refer to Table 2.3). Comparing them with cell 3, the other S Group cell, they have both larger diameters and more cilia. It has been established that having additional cilia can increase stiffness, but the increased cilia diameters might also play a role. As a brief exploration of the possible effect of cilia diameter on bundle stiffness, I tested an alternate "version" of cell 4 and compared it with the previous results. In the second version, the kinocilium diameter was decreased from 0.35 to 0.32 μm and the stereocilia diameter was decreased from 0.30 to 0.27 μm (roughly 10% decreases). To keep the tip and side link lengths constant

(reducing the number of independent variables) the locations of the cilia were moved closer together by scaling coordinates. Using this technique, the general configuration of the bundle was maintained.

The resulting decrease in stiffness was significant. The approximately 10% decrease in cilia diameters resulted in about a 20% decrease in stiffness. Although this has not been studied at length, it is interesting to note that a 10% decrease in diameter is equivalent to an 19% decrease in stereocilia cross- sectional area; thus, the decrease in stiffness is roughly proportional to the decrease in area.

Effect of Increased Tip Link Modulus

A key unknown property for bundles is the value of the tip link elastic modulus (E_{tl}). As has been mentioned, it is generally accepted that the upper and lower limits of a reasonable estimate are elastin's $6x10^5$ N/m^2 and collagen's $1x10^9$ N/m^2, respectively. To investigate the effects of tip link modulus on bundle response, I ran a parametric series of tests in which the tip link modulus was varied from 10^5 N/m^2 to 10^{13} N/m^2 (note that this is outside the "reasonable" range). I tested one cell from C Group (Cell 1) and one cell from S Group (cell 4).

Figure 3.4 shows the stiffness vs. deflection plots for Cell 1. In general, and unsurprisingly, an increase in E_{tl} produces an increase in bundle stiffness. However, note that as E_{tl} gets very low or very high, further decreases of magnitude (when low) or increases of magnitude (when high) produce virtually no change in bundle stiffness, especially at higher deflections. There is a region between $1x10^7$ and $1x10^9$ N/m^2 where changes in E_{tl} (holding other variables constant) do cause large changes in bundle stiffness, though, and interestingly enough, this region falls into the "reasonable" region of moduli. Consequently, varying the value chosen for E_{tl} can have significant impact even if the value is restricted to being within the "reasonable limits." Similar results were found for Cell 4.

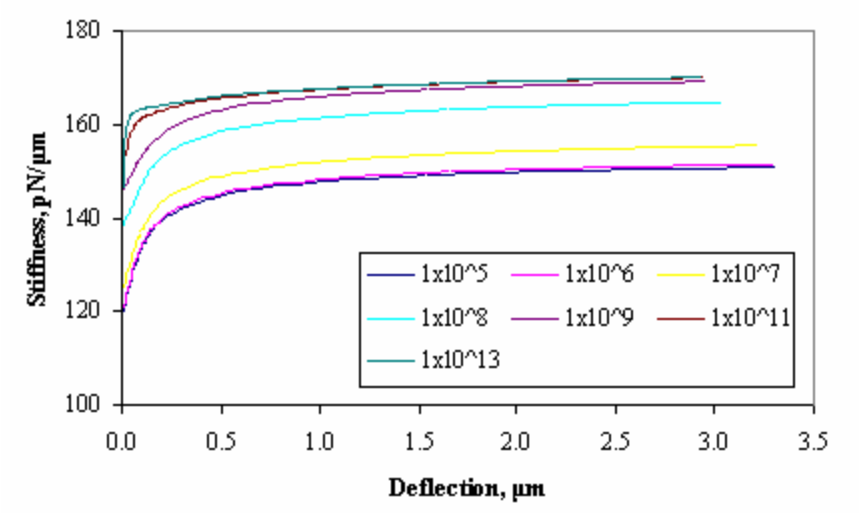

Figure 3.4: Cell 1 bundle stiffness for different E_{TL} values

More interesting than the stiffness plots, though, is the effect of E_{tl} on the tip link tension distribution. Before presenting this result, however, it is necessary to briefly digress and discuss serial and parallel theories of tip link tension distribution.

Since it is very difficult and presently impossible to measure tip link tensions in biological bundles, knowledge of tip link tensions primarily comes from modeling. Two alternative theories as to tip link distribution have arisen in the literature; these theories will be referred to as "parallel" and "serial" in this document. According to the parallel theory, tip links act essentially as rigid connectors and all tip links in a bundle have approximately the same tension at the same time. According to the serial theory, tip link tensions decrease as one moves along a row of stereocilia away from the kinocilium (Flock & Orman, 1983; Flock & Strelioff, 1984; Pickles, et al., 1984).

With this controversy in mind, examine Figure 3.5, which shows the tip link tension distributions for 4 values of E_{tl}: $1x10^6$, $1x10^7$, $1x10^8$, and $1x10^9$ N/m^2; these values span the "reasonable" region of values. The tip link tensions have been normalized by the highest tension value in the bundle; thus all tensions range from 0 to 1.

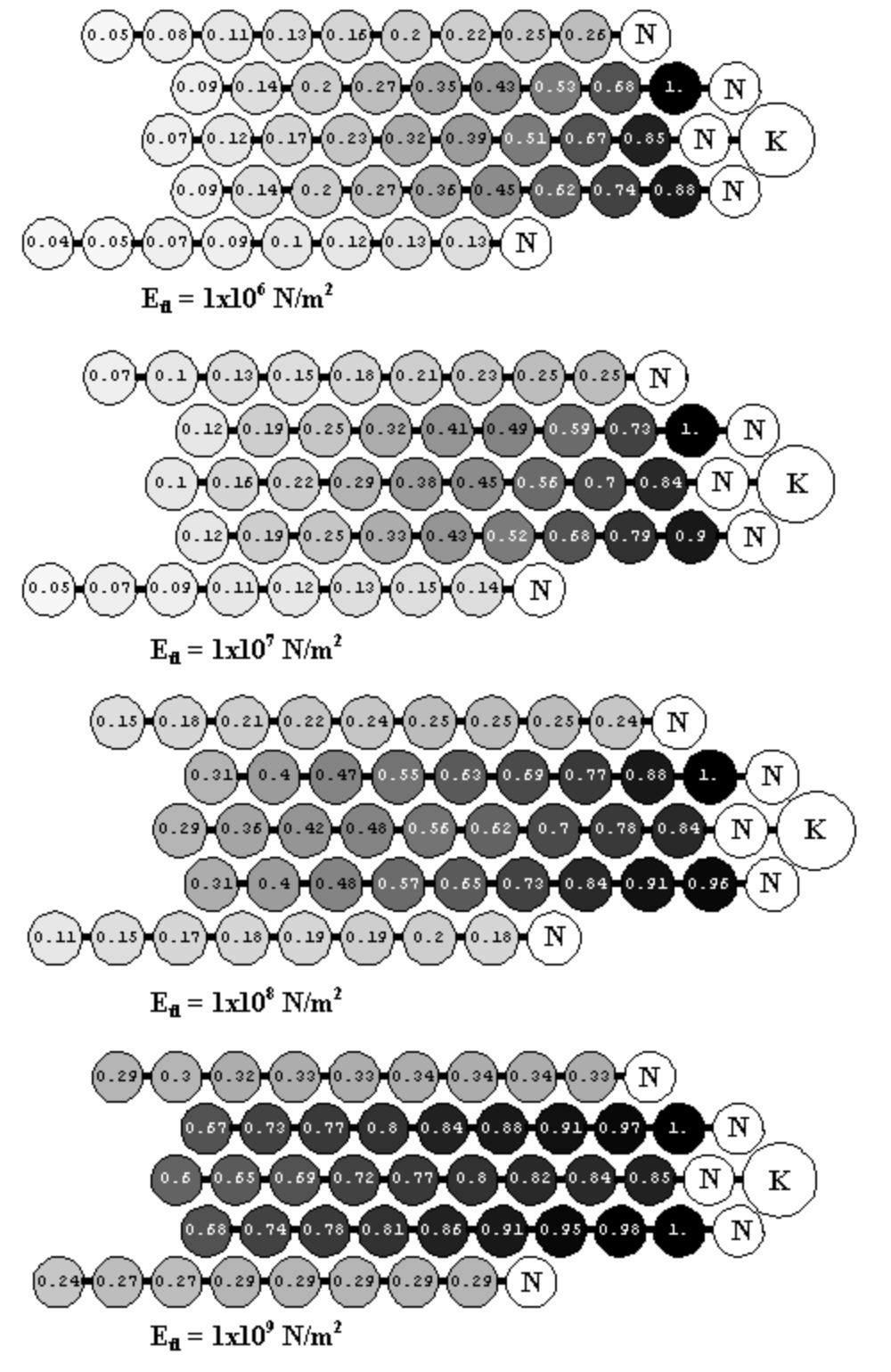

Figure 3.5: Circle tension plots for Cell 1 at varying E_{TL} values

This normalization allows for easier comparison between the cases, as increasing E_{tl} increases the absolute magnitude of tip link tensions.

Notice how the distribution of normalized tensions changes as E_{tl} is increased. At $E_{tl} = 1x10^6$, a serial tension distribution is clearly evident. Tensions are highest close to the kinocilium, and drop off steadily as one moves away from the kinocilium. The highest tensions, and the steepest drop off, are found in the middle three rows. As E_{tl} increases, the rate of drop off of tensions decreases; the difference in normalized tension between a tip link far from the kinocilium and one close to the kinocilium (assuming they are in the same row) becomes much less. The serial behavior is becoming less distinct. Careful observation of the top and bottom rows, though, reveals a more astonishing result: parallel behavior. At $E_{tl} = 1x10^9$ N/m^2, there is essentially no decrease in tip link tensions in the outermost rows as one moves away from the kinocilium, yet there is distinctive serial behavior in the three core rows. In fact, this disparity is really just a continuation of the trend seen even at $E_{tl} = 1x10^6$ N/m^2: the distribution of tensions in the middle three rows is more serial than the distribution in the outer two rows (or, likewise, the distribution in the outer rows is more parallel).

Figure 3.6 shows plots for Cell 4 at Etl = $1x10^7$ and $1x10^9$ N/m^2. One can observe a similar distribution as for Cell 1: the core three rows have the highest tensions and the most serial behavior, while the outer rows have lower tensions and more parallel behavior. In Cell 4's case, the outermost rows exhibit a fair amount of parallel behavior even at lower E_{tl} values, so the increased parallel behavior in the outer rows as E_{tl} is increased is less distinct but still present. The trend toward parallel behavior in the inner rows as E_{tl} increases is also present: note how the normalized tensions in the leftmost tip links more than double when E_{tl} is increased. Again, though, the core rows continue to exhibit a noticeable drop in tension as one moves away from the kinocilium. Revisit Figure 3.1 to see how this serial/parallel dichotomy was present, to varying extent, in all six cells with Etl = $1x10^7$ N/m^2.

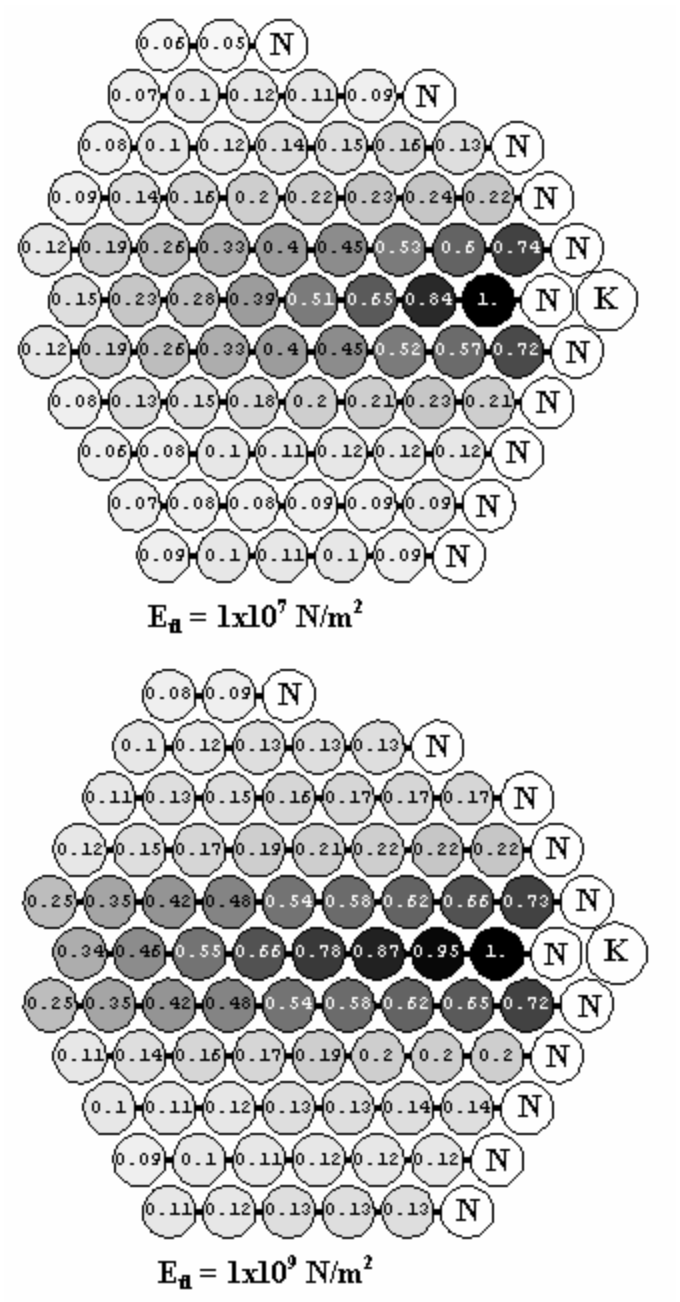

Figure 3.6: Circle tension plots for Cell 4 at two different values of E_{TL}

These results suggest that perhaps neither the parallel nor the serial hypotheses are correct; perhaps actual tip link tension distributions are a combination of the two, with inner rows exhibiting serial behavior and outer rows exhibiting parallel behavior. If this dual behavior occurs in real cells, then it strongly suggests that modeling bundles as stereocilia-in-a-row, rather than three-dimensionally, is leaving out important aspects of

bundle behavior. Also, the degree of parallelism that a real bundle exhibits is related to its E_{tl} value. The more parallel the behavior, the higher the value of E_{tl}.

Another implication relates to experimental practice. It may not be sufficient to merely examine the outermost row of a real bundle (i.e. by looking at the bundle from the side, which may be done out of convenience); the inner rows may be exhibiting markedly different behavior.

2-D vs. 3-D Comparison

Many models of cell bundles in the literature use a single row or column of stereocilia to represent an entire bundle, implicitly (or explicitly) assuming the response of the row will be similar to the response of a bundle.

To test the validity of such an assumption, I compared the response of the center row of cell (including the kinocilium) with the response of the entire cell, under the same loading conditions. The two cells tested were cell 1 (from C Group) and cell 4 (from S Group). The same loading conditions as described in the first part of this chapter (point load at kinocilium tip ranging from 1 to 500 pN) were applied, and stiffness plots and tip link tension distributions were collected.

Figure 3.7 shows stiffness vs. load plots for cell 1 and cell 4. Stiffness was plotted against load due to wide ranges in deflection for cell 4. The most significant difference is that the stiffness is virtually constant for the single rows (less than a 1% change), while the full bundles increase stiffness significantly (24% for cell 1; over 50% for cell 4). Also of note is that for cell 4, even the initial stiffness of the bundle is 3 times that of the lone row, and the disparity widens as the stiffness of the bundle grows. The stiffness difference in cell 1 between the two cases is less, but still noticeable.

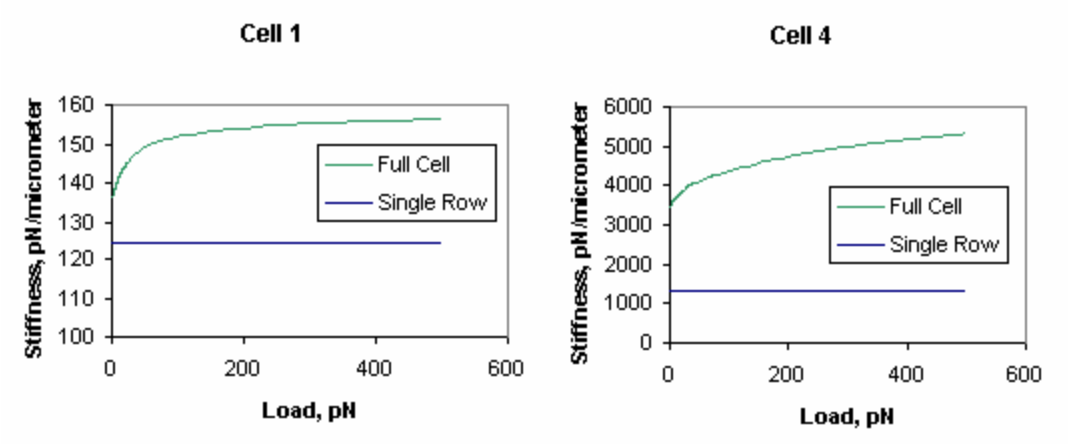

Figure 3.7: Stiffness vs. load plots comparing full cell & single row

Figure 3.8 shows tension circle plots for cell 1 and cell 4 full bundles and single rows. The main point of interest is that tensions in the lone row are much higher than the tensions in the middle row of the full bundle. In the case of cell 4, the tensions are up to 3 times as high! However, all cases still exhibit serial behavior.

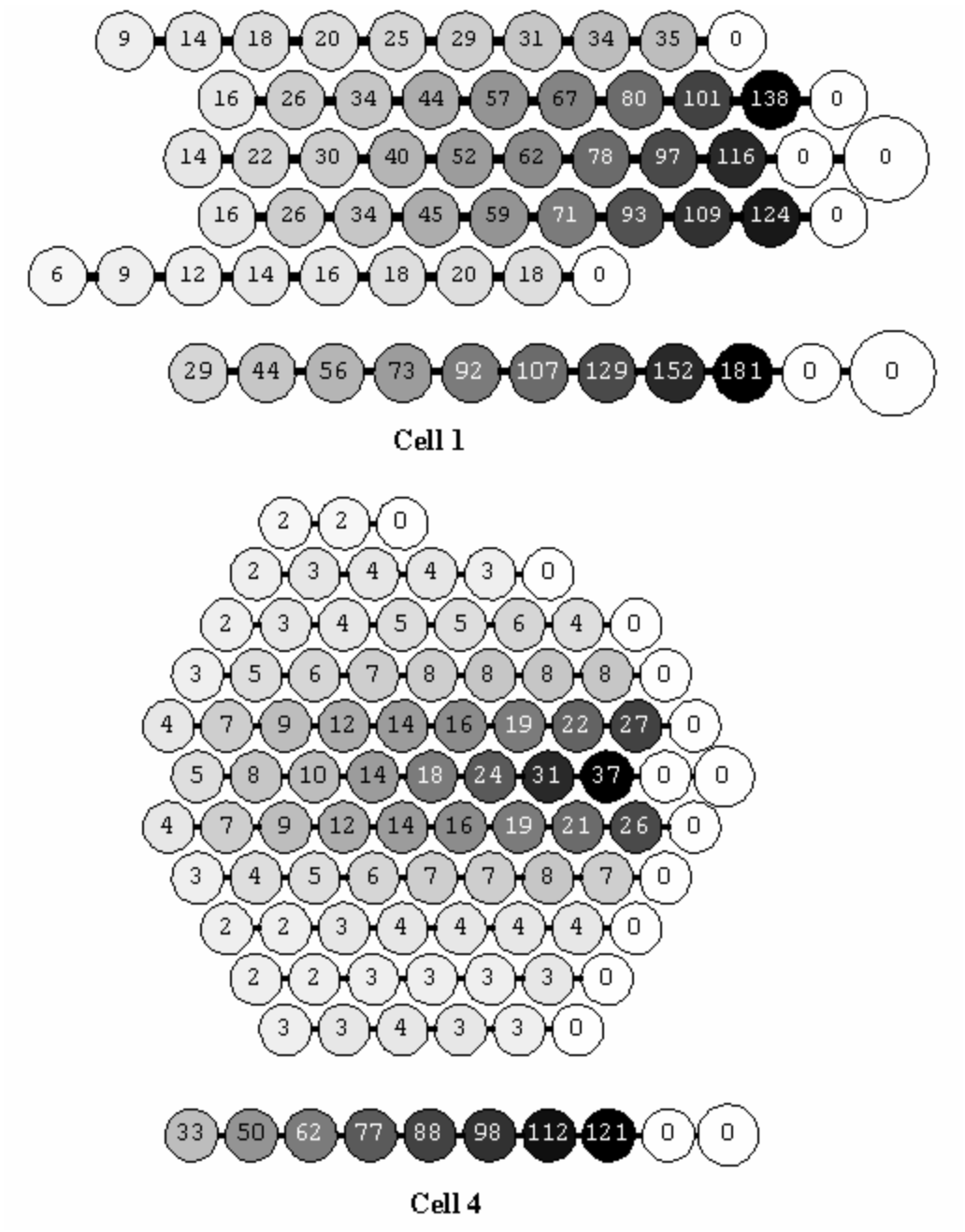

Figure 3.8: Tension circle plots for full cells and single rows, cells 1 & 4

These results have interesting implications. The fact that stiffness is virtually constant across a range of loads/deflections for the lone rows, but increases significantly for the full bundle, suggests that the other rows gradually come into play as the load increases. This implication supports the "recruitment" theory; the single row version of the bundle doesn't have any side rows to recruit, and so cannot increase stiffness significantly.

These results also support the idea that stereocilia to kinocilium height ratios are important in determining stiffness; note that while the cell 4 row had 1 fewer stereocilium than the cell 1 row, it had a stiffness approximately 10 times that of the cell 1 row. Clearly, the number of cilia is not the issue here. As a caveat, it is worth recalling that the stereocilia in cell 4 do have larger diameters than those in cell 1, but it is also worth recalling that based on the diameter-modifying experiment, the diameter difference is not likely to be responsible for more than a small portion of the difference.

One possible explanation for the increased tip link tensions involves energy distribution. In the full bundle, there are many more stereocilia and links to distribute energy to (energy being provided by the applied load). In the single row, there are much fewer cilia and links; therefore, one would expect greater deformations and/or higher tensions.

The overall conclusion that one can come to from this experiment is that representing a bundle as a single row or column can lead to misleading results; it neglects the changes in stiffness that occur, can underestimate the stiffness, and will overestimate the tip link tensions for a given load. It also neglects the difference in tip link tension distribution between the inner rows (serial) and outer rows (parallel), as shown earlier in this chapter.

Effect of Distributed Load

The last topic for this chapter involves comparison of bundle loading methods. Two methods are commonly used to deform bundles experimentally. One method is to push or pull on the kinocilium directly, such as with a fine glass whisker. The other method is to use a fluid jet directed at the bundle, which distributes the force more evenly.

In a simple experiment to compare the two types of loading, three cases were run on Cell 5, one of the "S Group" cells. The fluid jet was simulated by a distributed series of 9 point loads running the length of the kinocilium, linearly decreasing from a maximum at the tip to a minimum at the base. Two types of point loading were tested, both located at the kinocilium tip. In the first case, an equivalent force was applied, determined by summing up the 9 distributed point loads. In the second case, a force

generating an equivalent moment was applied at the tip, calculated by summing up the 9 moments from the distributed case and dividing by the height of the kinocilium. Figure 3.7 illustrates both point loading and distributed loading.

Stiffness of a bundle is generally defined by the load divided by the distance the kinocilium tip is deflected. This definition does not apply well to a distributed load; therefore stiffness-deflection curves were not computed. Instead, the deformed profile of the kinocilium was plotted for all three cases, and is shown in Figure 3.9. The deformations have been exaggerated for clarity by utilizing different X and Y scales.

Unsurprisingly, the distributed case showed a more even, linear distribution while the point load cases exhibited deformations that are fairly typical for a cantilever beam under a point load. The distributed load also resulted in a smaller kinocilium tip deflection than either of the point loads.

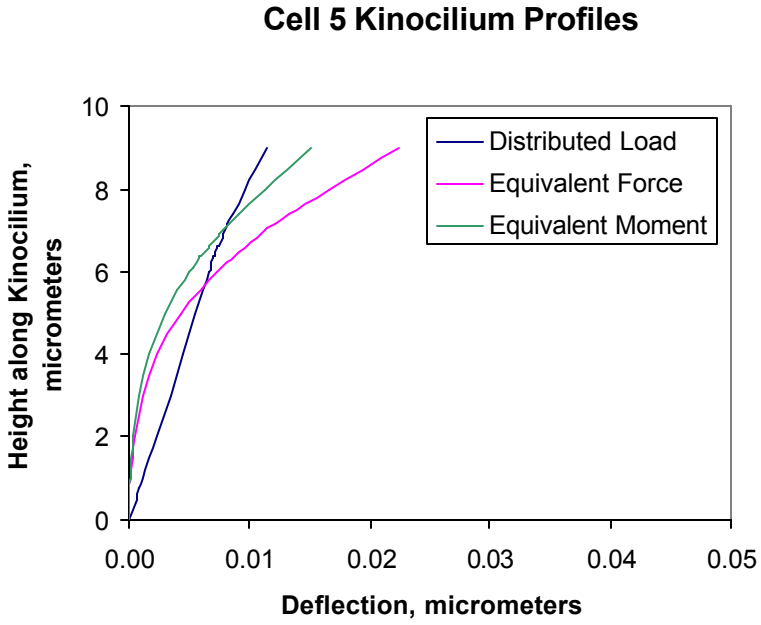

Figure 3.9: Kinocilium deformed profile under varied loading conditions

Summary/Conclusions

Several interesting conclusions came out of these results. Most are discussed in the sections involving them, but key concepts are summarized as follows:

1) ***3-D bundles exhibit dual parallel/serial behavior, with a tendency toward increased parallelism as tip link elastic modulus is increased***. This result supports the conclusion that 2-D modeling is insufficient to capture all the important aspects of cell behavior; it also suggests that merely looking at a side row of a bundle experimentally may be insufficient as well.
2) ***Stereocilia/kinocilium height ratios are the most important factor in determining bundle stiffness as well as in determining tip link tensions***. I suggested that the stiffness effect is due to the stereocilia anchoring the kinocilium at a higher position, leaving less of it to freely bend. The inverse nature of the tip link tension variation (taller stereocilia = lower tension) may be a "lever" effect; the taller stereocilia have a larger moment arm, so less of a force (i.e. tension in the tip links) is needed to produce the same moment. However, when individual rows from cell 1 and cell 4 were examined, much less difference in tip link tensions between the two cells was observed, so the cause/effect relationship may be more complicated.
3) ***Stiffness varies with load in three-dimensional bundles, but is essentially constant in a two-dimensional bundle***. As was mentioned, this result suggests support for the recruitment concept, in which stereocilia off the main column are pulled in to stiffen the bundle as the applied load increases. This result also suggests that 2-D modeling is not adequate to accurately describe bundle behavior.
4) ***Modeling bundles as a single row of cilia does not provide accurate and complete results***. Bundle stiffness values, tip link tension values, the non-constant bundle stiffness behavior, and the serial/parallel dichotomy are all changed or lost when reducing a bundle to a single row.

CHAPTER 4: ION GATES

Recall from the introduction that it is believed that tension-gated ion channels are responsible for current flow in hair cell bundles, as well as causing the mechanical effect of a drop in bundle stiffness. Experimentally, this drop in stiffness has been shown to be in the range of 20-40% (calculated from Howard & Hudspeth, 1987). Although there is some disagreement in the literature as to the exact mechanism, it is widely agreed that increased tension in the tip links induces some mechanism to relax the tip link tension, thus reducing overall bundle stiffness. Research discussed in this chapter involves my efforts to incorporate into the *bmod* program a model of these ion gates, reducing tip link tension when the gates open. In addition, I incorporated and tested the effects of a variable tip link elastic modulus, as well as pre-tensioning of tip links.

Tip Link Ion Gates

Procedure

Since *bmod* is a static response program, utilizing tension-based probability functions to open gates for a certain percentage of the time was not feasible. Instead, I opted to set a tension threshold so that any tip link having tension greater than or equal to the threshold would open its ion gate. To prevent oscillatory responses (with respect to program iterations, not oscillatory in time), gates are "locked" open after opening; that is, if a gate opens at one force step, and the tension in its tip link subsequently drops, the gate does not re-close. Without this feature, gates tended to open on one program iteration, close on the next, then re-open, and so on. This oscillatory behavior prevented the program from converging, and made obtaining useful results impossible.

To create the relaxation in the link, the opening of an ion gate causes the tip link's un-deformed length to increase by a gating distance "d" (Howard & Hudspeth, 1988). This increase could be due to a protein conformational (configuration) change and/or molecular motor slippage. The increase causes a resultant decrease in the strain of the link, and thus the tension decreases. Since the decreased length could cause the link to go into compression, I added a "tip link slackening" feature to *bmod* as well, similar to the lateral link buckling feature; the loads caused by tip links in compression are removed

from the system. However, tip links were allowed to re-tense if the geometry of the system deformed appropriately at higher loads (whereas lateral links are removed permanently).

To test the effect of the ion gates, I used the same six cells from Chapter 3, and compared the results with ion gates to the results obtained using the original version of the *bmod* program. The value of the gating distance "d" used (except where otherwise specified) was 4 nm, as suggested by Howard & Hudspeth, 1988.

Results

Figure 4.1 shows stiffness-deflection curves for all 6 cells, with $E_{tl} = 1x10^7$ N/m^2. Two curves are shown for each cell: a curve obtained as in Chapter 3, with no ion gates or tip link slackening, and a curve obtained using the model modifications described above. It can be easily observed that as the deflection increases, the stiffness of the "gates" case drops below the stiffness of the "no gates" case. The maximum percentage decrease from the "no gates" case to the "gates" case is on the order of 1 to 4%, depending on the cell, with Cell 4 having the largest drop and Cell 6 having the smallest. Figure 4.2 shows a similar set of curves, only now E_{tl} has been increased to $5x10^7$ N/m^2. Two qualitative differences can be observed between 4.2 and 4.1. First, the differences between the gated and un-gated cases are more noticeable when $E_{tl} = 5x10^7$ N/m^2, in Figure 4.2. The maximum percentage decrease from "no gates" to "gates" varies from 3% (Cell 6) to about 13% (Cell 4), a much higher difference than in the previous case. Second, the manner in which the gated curve "drops off" is different. In Figure 4.1 ($E_{tl} = 1x10^7$ N/m^2), both curves lie atop one another for a certain way, and then the gated curve slowly drops off. In Figure 4.2 ($E_{tl} = 5x10^7$ N/m^2), the gated curve drops sharply at a very low deflection (the exception being Cell 3, which behaves the same way as in Figure 4.1).

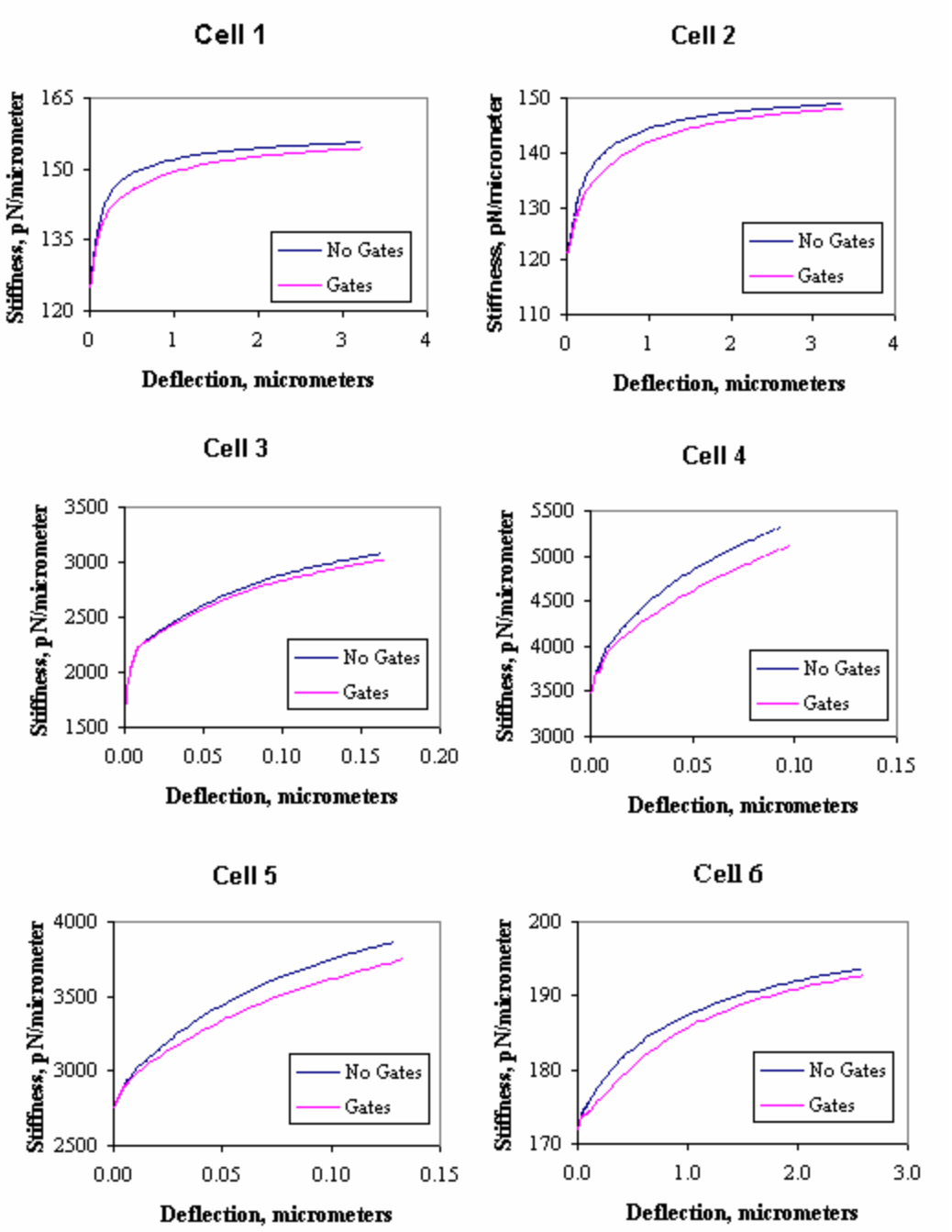

Figure 4.1: Stiffness comparison at $E_{t1} = 1x10^7$ N/m^2

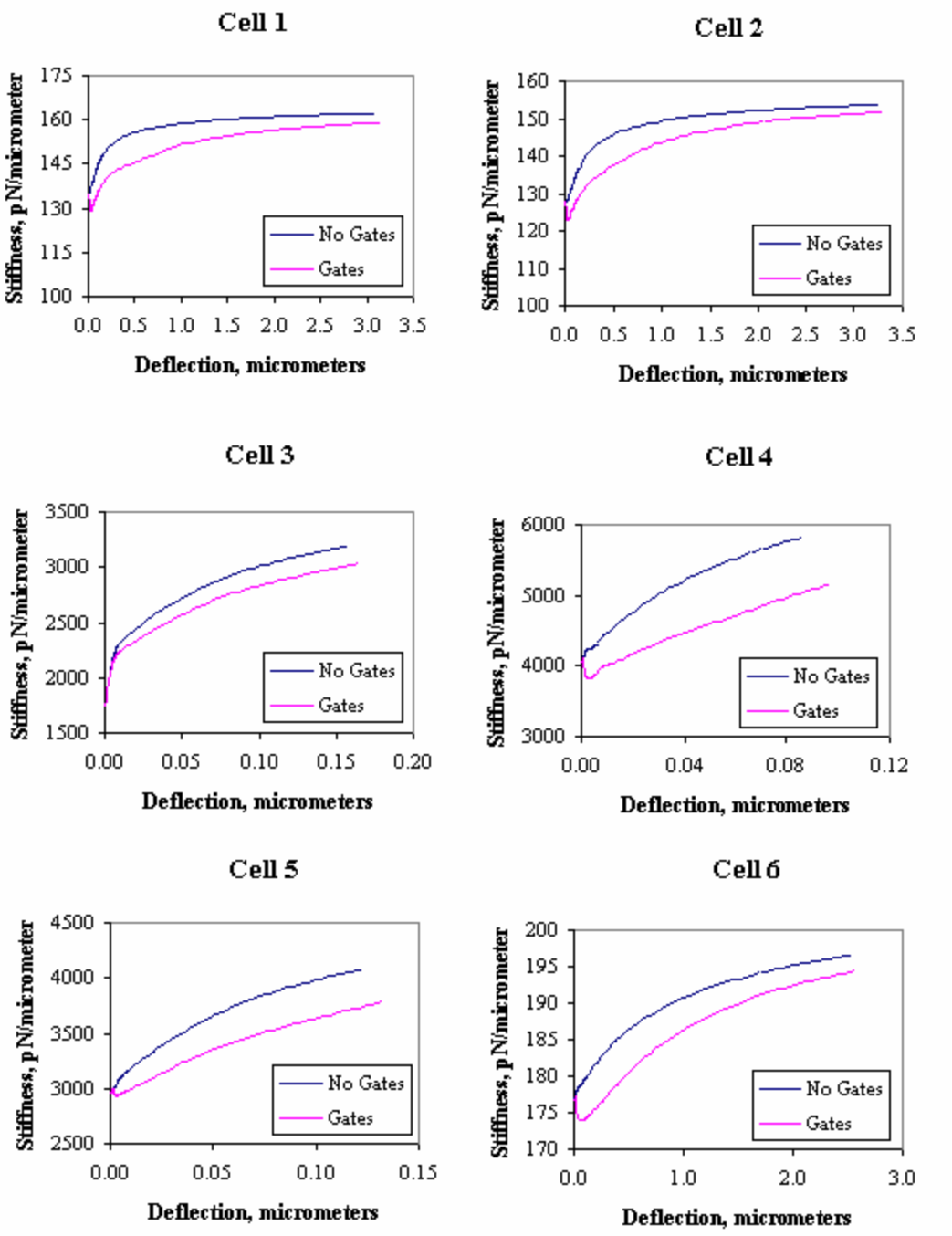

Figure 4.2: Stiffness comparison at $E_{tl} = 5x10^7$ N/m^2

Cell 1 and cell 4 (representatives of C Group and S Group) were tested at higher values of E_{tl}: $1x10^8$ N/m^2 and $5x10^8$ N/m^2. These results are shown in Figure 4.3. Stiffness drops continue to increase. Cell 1 has an 8% drop when $E_{tl} = 1x10^8$ N/m^2, and

cell 4 has a nearly 17% drop. When Etl = $5x10^8$ N/m^2, cell 1 has a 12% drop, and cell 4 has a 25% drop.

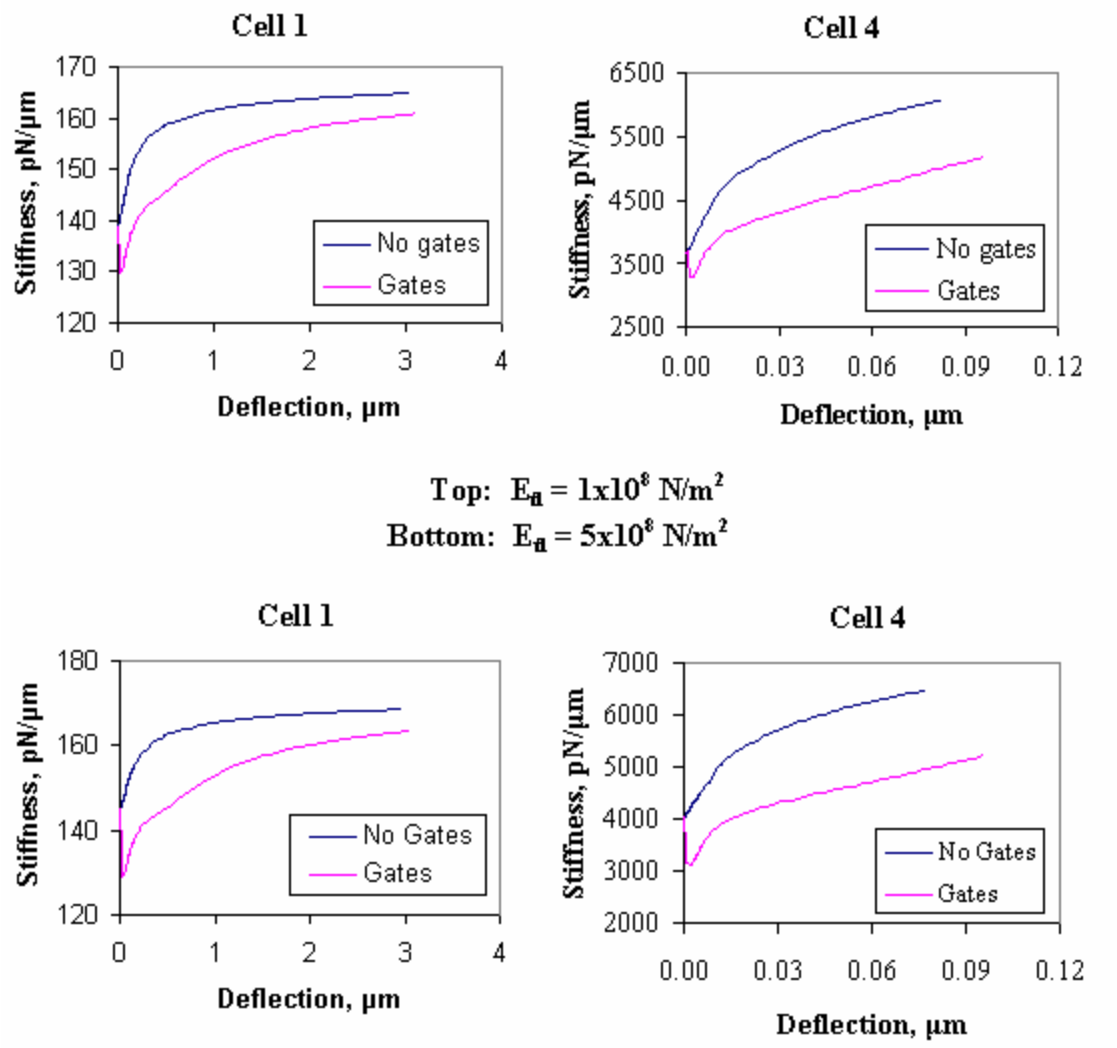

Figure 4.3: Stiffness comparison at higher E_{tl} values

Discussion

The decrease in stiffness is due to tip links going slack, which is in turn due to ion gates opening, and relaxing the tip links. In the first set of curves (E_{tl} = $1x10^7$ N/m^2), the opening of the ion gates is staggered; gates open a few at a time as the bundle load (and the tip link tension) increases. In the second set of curves (E_{tl} = $5x10^7$ N/m^2), the ion gates tend to open more in clumps, at smaller deflections, creating a sudden drop-off. Two factors are likely causes of this "clumping" of ion gate openings. First, higher elastic modulus in the tip links means higher absolute tip link tensions. This phenomenon has

shown up very consistently in all of the modeling efforts described in this paper. Higher tensions mean that the ion gates reach threshold tension sooner, and thus the opening of ion gates are clustered at lower force levels. Second, higher elastic modulus means tip link tensions are more "parallel" in behavior, increasing the likelihood that multiple tip links will hit threshold under the same force load.

Not only is the drop-off more sudden in the second set of curves, but it is greater, because the tip links are carrying a higher load. Complete slackening of the tip links (so that they carry no load) results in the greatest possible drop in load and a greater stiffness drop for the bundle than if the links merely reduced their tension. Howard & Hudspeth (1988) suggested that the sharp stiffness drops they observed might be due to tip links buckling under compression. The results I obtained also seem to suggest that if the opening of ion gates causes a significant drop in bundle stiffness, tip links must be relatively stiff.

The main result of interest for the higher values of E_{tl} is that the percent stiffness drop continues to rise, up to 25% for cell 4. These results show that stiffness drops in the 20-40% realm as observed by Howard and Hudspeth are achievable using this model and that if such drops occur, the tip link elastic modulus must at least in the upper realm of the reasonable region (recall that $1x10^9$ N/m^2 is the value of collagen and the upper limit for tip links).

It should also be noted that Howard & Hudspeth utilized bullfrog cell bundles, which have a very different geometric arrangement from turtle cell bundles. Bullfrog cell bundles resemble a rounded cone, with the stereocilia all tilted in towards the bundle center. Even among the six turtle cell bundles studied, varying stiffness drops were achieved due to structural differences; therefore, it seems reasonable that structural differences could account for Howard & Hudspeth measuring larger drops than were achieved using *bmod*.

Effect of Gating Distance on Stiffness Drop

In all the tested cases so far, the drop in tension was directly due to tip link slackening. An important question to answer would be this: is it possible to achieve significant tension drops without the slackening? I ran a series of tests in which the

gating value "d" was decreased in an attempt to answer this question. The stiffness results for cell 1 and cell 4 for several cases are shown in Figure 4.4. All cases were run with E_{tl} = 5x10^7 N/m^2.

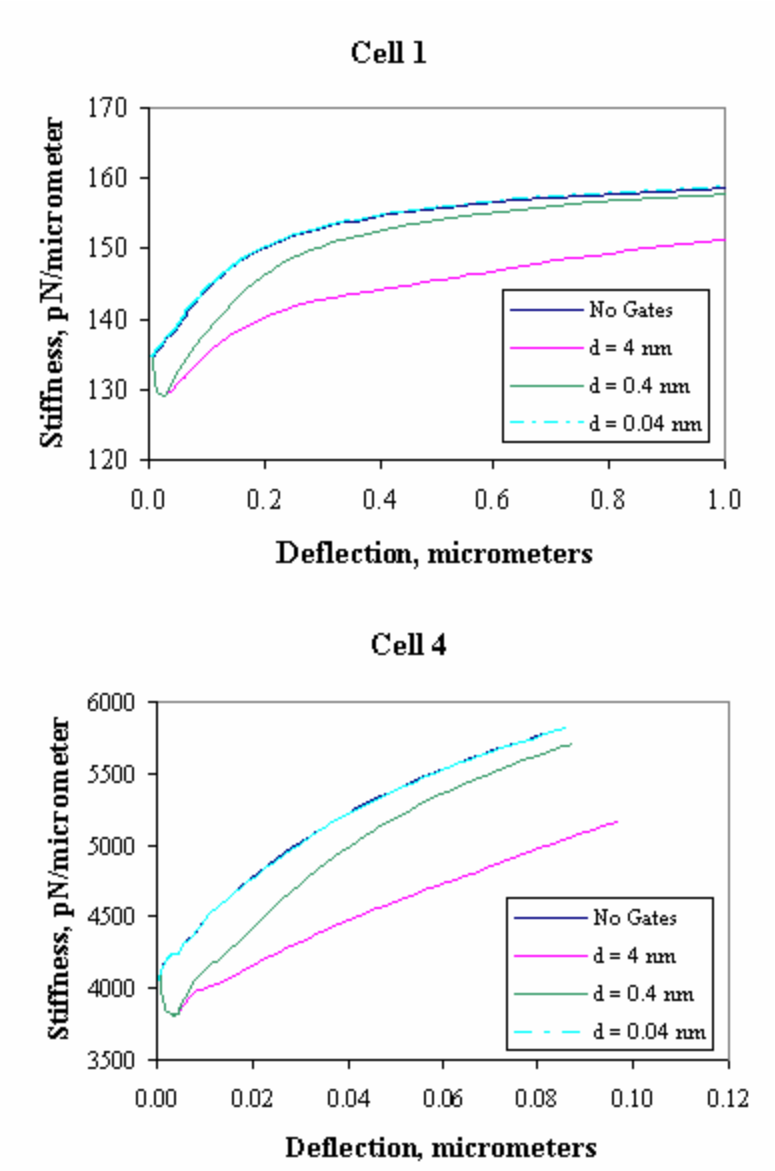

Figure 4.4: Effect of ion gating distance "d" on bundle stiffness

Trials for three "d" values are shown in Figure 4.3: 4 nm, 0.4 nm, and 0.04 nm. Recall that in the earlier trials, a value of 4 nm was used. In the cases of 4 nm and 0.4 nm, tip link slackening occurred, while in the case of 0.04 nm, it did not occur. I confirmed through trial and error that the largest gating distance possible without causing

tip link slackening is somewhere between 0.04 nm and 0.05 nm. Therefore, 0.04 nm is a good approximation as to the largest gating distance that can be achieved without tip links going slack.

From the graphs, it is clear that for both cell 1 and cell 4, the 0.04 nm case exhibited essentially no change in stiffness with respect to the no-ion-gates case, while the two cases that incurred tip link slackening did show a substantial decrease in stiffness. Since a value of d = 0.04 nm is the upper boundary for preventing tip links from going completely slack, yet still too low for noticeable stiffness drops, these results strongly suggest that tip links must go slack in order to cause bundle stiffness to drop.

Nonlinear Tip Link Response

I experimented with two other sophisticated additions to *bmod*: variable tip link modulus, and pre-tensioning. Making the tip link modulus variable was a simple way to approximate a non-linear response in the tip links. Most biological materials do not have a simple linear stress-strain relationship, but rather one which looks more like an exponential curve, or a power curve; therefore I used an exponential function similar to the following:

$$E_{TL} = E_{TLBASE} \times e^{ke}$$

where E_{tlbase} is the initial elastic modulus (at 0 strain), e is the number whose natural log is 1, k is a constant that controls the rate of strain-hardening, and e is the strain in the tip link. This formula was used to "update" the elastic modulus of each tip link every time the stiffness matrix was calculated by the program. Thus, at every force step or iteration, a new tip link modulus was calculated, and could be different for each tip link. In the event that a link slackened or went into compression, E_{tl} was reset to the base value.

Recent research (Kachar, et al., 2000) has suggested that tip links might be similar to elastic proteins such as titin. For this experiment, the value of **k** used was 25; this value was obtained by curve-fitting data for titin reported by Tskovrebova, et al., 1997. The base value of E_{tl} is the same as was used in most of Chapter 3: 1×10^7 N/m^2. Figure 4.5 shows a plot of the E_{tl} function for these parameters.

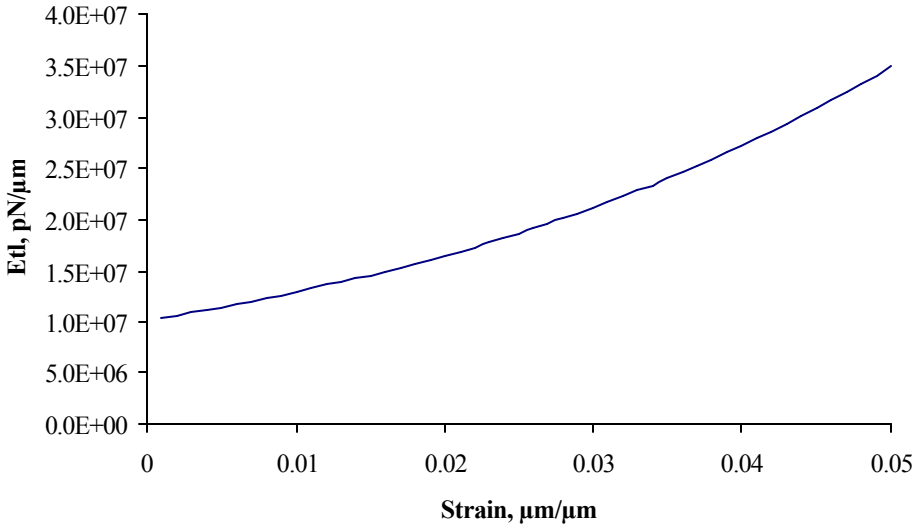

Figure 4.5: E_{tl} as a function of strain

Figure 4.6a shows stiffness plots for cell 1 and cell 4 using this stress-strain relationship. Ion gates were not utilized in this comparison.

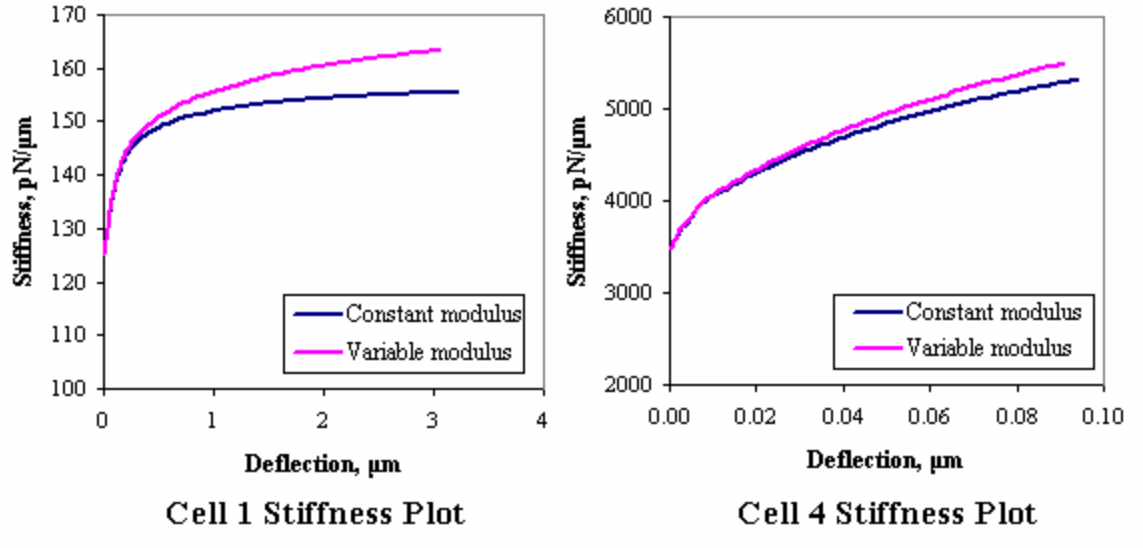

Figure 4.6a: Variable modulus comparison without ion gates

The inclusion of the variable tip link modulus resulted in little change at low deflections, but a noticeable increase in stiffness at higher deflections. This result was expected, as higher bundle deflections cause higher strains in tip links, which in turn result in stiffer tip links due to the strain-hardening elastic modulus.

To better compare cell 1 against cell 4, examine Figure 4.6b, which shows normalized bundle stiffness vs. applied load. The normalized bundle stiffness was obtained by dividing the variable case stiffness by the constant case stiffness at each point. For example, a normalized stiffness of 1.02 under a given load means that the cell with variable tip link modulus had a bundle stiffness 1.02 times that of the same cell with constant modulus, at that force load. Interestingly, the smaller cell, cell 1, showed a noticeably higher normalized stiffness than cell 4, which suggests that its tip links increased their elastic modulus more than the tip links in cell 4. Since E_{tl} is a function of strain, the higher normalized stiffness in cell 1 ultimately implies that cell 1's tip links were undergoing higher amounts of strain than those in cell 4.

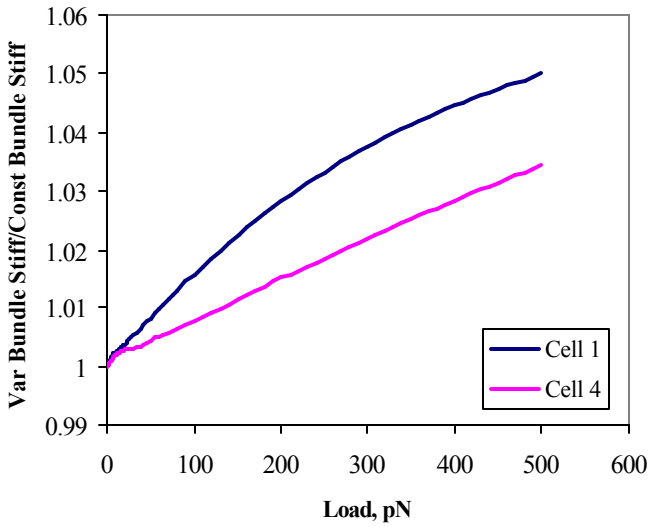

Figure 4.6b: Normalized stiffness comparison

These implications are confirmed by quantifying the changes in E_{tl} for each cell. The tip link modulus for both these cells started at $1x10^7$ N/m^2 when the cell was under no load. Under a 500 pN load, the average value of E_{tl} for cell 1 was $1.6x10^8$ N/m^2, while the average value of E_{tl} for cell 4 was $2.1x10^7$ N/m^2. Using the formula for E_{tl} as a function of strain given earlier, the average strain e for cell 1 was 0.11 µm/µm, while the average strain for cell 4 was 0.03 µm/µm.

I was able to confirm that a similar discrepancy in tip link strains between the two cells occurred even when the elastic modulus was constant. One possible explanation is

that because cell 4 is so much stiffer than cell 1, the bundle as a whole is deflected less, and consequently each tip link in cell 4 is strained less.

Figures 4.6a and 4.6b both utilized models lacking the ion gates feature. For the next set of plots, Figures 4.7a and 4.7b, ion gates, as described earlier in this chapter, were implemented. The gating distance d was 4 nm, and the ion gate opening threshold was 3 pN. E_{tl} was $1x10^7$ N/m^2 for the constant cases, and again was the base value for the variable modulus cases). In Figure 4.7a, the plots compare cell 1's stiffness with and without ion gates. The left plot shows results using a variable modulus; the right plot shows results using a constant modulus.

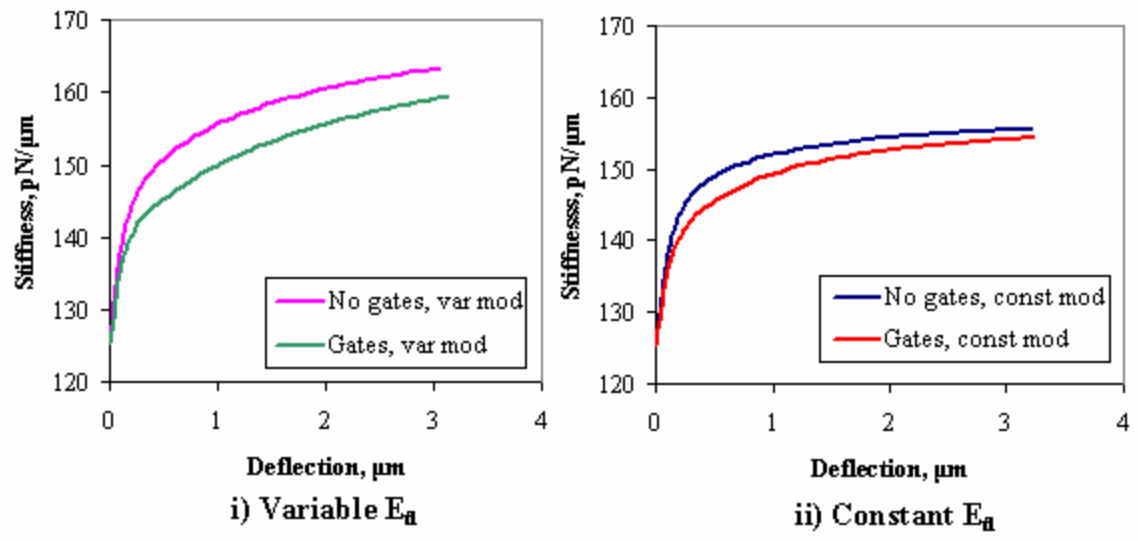

Figure 4.7a: Ion gate comparison, cell 1

The main observation of interest for this pair of plots is that the difference between ion gates and no ion gates is much larger when the tip links have a variable modulus. Also, this difference does not decrease much under large deflections; in contrast, if the modulus is constant, the two stiffness values (gates and no-gates) tend to converge as deflections get large. Now examine Figure 4.7b, which shows the same pair of plots for cell 4.

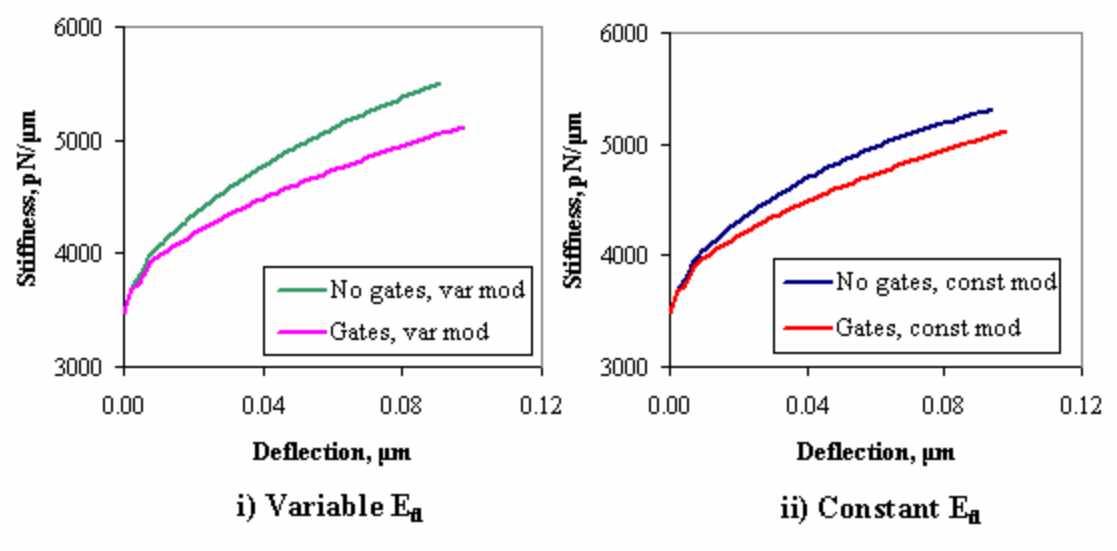

Figure 4.7b: Ion gate comparison, cell 4

Again, when the tip link modulus is variable, the disparity between the gates and no-gates cases is wider. Also, the disparity is continually widening when E_{tl} is variable, while in the case where it is constant, the disparity levels out and does not widen further at large deflections. Calculations of the percent stiffness drop between the gates/no-gates cases yields a maximum drop of 6.9% for the variable case, where the constant modulus case had a maximum drop of 3.9%. Clearly, the variable elastic modulus had a significant effect on the amount of stiffness drop.

As a final experiment in this section, I compared gates and no-gates cases for cell 4 with $E_{tl} = 5 \times 10^7$. Recall from earlier in the chapter that the stiffness drop between gates and no-gates cases was found to be 13% for cell 4 with that value of E_{tl}. However, adding the variable elastic modulus did not change the maximum stiffness drop by any significant amount. 13% was still the maximum drop I could obtain.

In summary, the two main mechanical effects of the variable tip link modulus were an increase in bundle stiffness which grew as the applied load was increased, and a greater stiffness drop from ion gates opening (at least in some cases).

Pre-tensioning

The other feature investigated was pre-tensioning. It is believed that in real cells, molecular motors act to keep tip links under a small but significant amount of tension

even in the absence of an externally applied load. This "pre-tensioning" is believed to be responsible for a resting current of the cell, again observed under the absence of an external load. This change was implemented by modifying the un-stretched length of each tip link so as to be smaller than the distance between its two points of attachment. Thus, even without deformation of the bundle, the tip link would be strained, and carry a tension.

The implementation was successful. No unusual results occurred that suggested that pre-tensioning was mechanically unrealistic. However, the pre-tensioning had no readily discernible influence on the bundle, other than to enable tip links to reach their threshold tensions sooner (because they started from a non-zero tension). For this reason, pre-tensioning was not further investigated.

Other Factors

As part of the learning process in this part of the research, other properties than just the elastic modulus of the tip links and the value of the gating distance were investigated. For example, more careful research on tip link diameters led to a decision to increase the tip link diameter from 5 nm to 10 nm (Kachar et al., 2000; Tsuprun & Santi, 2002). This change resulted in a significant increase in tip link cross-sectional area, and allowed the tip links to carry a higher load. Another modification from early methods was to increase the amount of tapering at the stereocilium base; that is, make the base diameter smaller relative to the main diameter. Prior to the change, a ratio of ½ was used, meaning the base diameter was ½ the size of the main diameter; this ratio was changed to 1/6 based on scaled images from electron microscopy (Peterson, 2002; Flock, 1965; Tilney et al., 1983) that showed a sharp narrowing in diameter near the stereocilium base; visually, 1/6 seemed a better approximation than ½.

Both of these changes increased the amount of the stiffness drop, presumably because they resulted in tip links carrying a higher percentage of the total bundle load than previously. All of these changes were implemented prior to running the tests described in this thesis; however they are mentioned because they are yet another reminder that details are important in modeling, especially in this model.

Conclusions

In summary, there are two crucial factors in influencing the stiffness drop for a given cell (besides its geometric configuration). First, the tip links must buckle or go slack when the ion gates open. I was unable to achieve any significant drop in bundle stiffness when the tip link tension merely relaxed. In order for slackening to occur, the gating distance "d" must be sufficiently large ($d > 0.04$ nm). The second factor is the stiffness of the tip links. The stiffer the tip links, the higher load they carry, and thus the greater the stiffness drop if it goes slack.

Is the phenomenon of tip links going slack biologically realistic? Possibly. It seems reasonable that either a protein configuration change, a molecular motor slipping, or both, could cause a tip link to go slack, resulting in a decrease in bundle stiffness if enough links did so simultaneously. As time progressed, the molecular motor would re-tense the link. This behavior would allow the bundle to adapt to fixed deflections, and be ready to transduce the next disturbance.

Quantitatively, I was able to achieve stiffness drops of up to 25%, which is in the region of the 20 to 40% reported in the literature by Howard and Hudspeth. Cell 4 was the only bundle shown to be able to achieve such a drop, although cell 1 came close, and cells 2, 3, 5, and 6 were not tested at the higher E_{tl} levels. As mentioned before, Howard and Hudspeth utilized bullfrog hair cell bundles, whereas this research modeled turtle bundles. Lacking information on the specific differences between the hair cells in the two types of animals, it is difficult to say if a 20 to 40% figure would apply to a turtle. Based on visual observation, turtle and bullfrog bundles do differ in geometric arrangement. This research showed that bundle structure plays a significant role in the amount of stiffness drop, so experimental data on stiffness drops of turtle bundles (or modeling data for bullfrog bundles) is needed for any further comparison. If the higher stiffness drop figures obtained by Howard and Hudspeth do apply to turtle bundles, they provide support for the idea that tip links are fairly stiff and may have an elastic modulus somewhat close to collagen's 1×10^9 N/m^2.

The results of implementing a variable tip link modulus were somewhat inconclusive. Although the variable modulus clearly resulted in higher bundle stiffness (at large deflections), the effect on ion gate stiffness drops was more varied; in some of

the cases, it resulted in a much larger drop; in one case, it made virtually no difference. Implementation of pre-tensioning seemed to make no difference at all. However, it should also be noted that nothing in the results obtained suggested that implementing these features caused results that are unrealistic or incompatible with accepted theory. Also, the failure to obtain much practical significance from these features does not mean that they are insignificant in actual bundles. The amounts of pre-tensioning, and rate of increase of tip link modulus were educated guesses; better estimates of these values might result in more significant results.

CHAPTER 5: CONCLUSIONS AND FUTURE WORK

If one were to try and sum up the conclusions obtained from this research into one statement, perhaps the best summary would be to say that bundles are mechanically complex, and all details are important in accurately modeling them.

Accurate knowledge of the geometry of a bundle is crucial. Cilia diameters, numbers of and locations of cilia, and cilia heights all have significant effects on bundles stiffness, as elaborated on in chapter 3. Although not discussed in detail, even factors such as stereocilia base tapering, and tip link diameters can noticeably influence stiffness. Certainly, modeling a bundle as a simple row or column neglects a significant amount of information and can give incorrect results.

Equally important in accurate modeling are the material properties, such as elastic moduli and shear moduli. Of particular importance is the tip link elastic modulus, which is important both in affecting overall bundle stiffness, as well as influencing the behavior of the theorized ion gated channels.

All of these factors are of extreme importance just in static response of bundles! The complexities of dynamic response are surely even more challenging and dependent on these (and other) factors.

The implications of these conclusions are three-fold. First, and unsurprisingly, better information about bundles is needed to improve modeling efforts. The material properties of tip and lateral links need to be known more precisely. Unfortunately, it is currently impossible to measure these properties directly; testing values in a model is presently the best possible way to determine these values. Geometric properties of individual bundles being modeled need to be measured more exactly. The details are important; rough estimates are insufficient. The importance of the stereocilia/kinocilium height ratio suggests that accurate height data is particularly crucial, but cilia diameters, taper ratios, and other values are also vital. Second, modeling needs to be as precise as possible. Lumped parameter models and simple 2-D row models are not sufficient. They may provide some useful information, but not enough. Two striking aspects of bundle response, namely the simultaneous serial/parallel behavior, and the non-constant bundle stiffness, would be lost in a 2-D row model. Three-dimensional finite element methods

(or equivalent) are needed for accuracy and completeness. Third, the ability of small variations to significantly influence bundle response implies the possibility of extensive specialization between bundles. All of the bundles studied in this research were thought with good certainty to be Type II vestibular bundles, yet a huge degree of variation was found between them. This variation suggests that merely categorizing vestibular cells into two types doesn't give the entire picture. Smaller variations, whether in cilia diameter, cilia arrangement, or other geometric factors, may allow different regions of the vestibular organs to pick up and transduce different types of information; for instance, a bundle's stiffness may determine the range of accelerations that it can detect and transducer. Some bundles might even be attuned to seismic vibrations. A complete understanding of the vestibular system would require knowledge and comprehension of such variations, and better techniques for obtaining the model input data in combination with more accurate modeling could eventually allow such an understanding.

In the future, the issue of lateral link buckling needs to be further examined. The fact that we had to remove lateral links to achieve realistic results means that either our model needs to be improved, or actual hair cell bundles are missing lateral links in certain locations. This buckling phenomenon needs further investigation at the experimental, anatomic, and modeling levels. In general, the current state of knowledge concerning links connecting stereocilia needs to be greatly improved at all levels.

The next major step in improving the *bmod* model is to make it dynamic and allow time-based responses. Such a drastic modification will allow the modeling of more complex aspects of bundles, such as adaptation, molecular motors, and realistic ion channel response. The work presented in chapter 4 confirmed that significant stiffness drops from ion gates' opening can be obtained, assuming tip link slackening occurs (and given a sufficiently high tip link modulus; again, more reasons why an accurate value is needed). Not much specific evidence for or against variable tip link modulus or pre-tensioning was found; the variable tip link modulus had some effects on bundle stiffness and ion gate stiffness drops, but the effects were fairly subtle. A better understanding of tip link material properties would allow for a more realistic approximation of tip link mechanical behavior, including stiffness variation. At that point in time, it might be worthwhile to include the tip link nonlinear behavior in the model.

References

Bagger-Sjoback, D, and M. Takumida. (1988) "Geometrical array of the vestibular sensory hair bundles". Acta otolaryngol (Stokh), 106: 394-403

Cotton, J. (1998) "Mechanical modeling of vestibular hair cell bundles." Doctoral dissertation, Virginia Tech.

Cotton, J.; Peterson E.H.; Grant, J.W. (1998) "Mechanical nonlinearities in deformation of hair cell ciliary bundles.", Twenty-first Midwinter Meeting of the Association for Research in Otolaryngology, St. Petersburg, FL, February 15-19, 1998

Cotton, J; Grant, J. W. "A finite element method for mechanical response of hair cell ciliary bundles." Transactions of the ASME. February 2000. 122: 44-50

Crawford A.C., Fettiplace R. (1985) "The mechanical properties of ciliary bundles of turtle cochlear hair cells." J Physiol Lond 364: 359-379.

DeRosier, David J; Tilney, Lewis G. (1984) "The form and function of actin: a product of its unique design." Cell and Muscle Motility. Vol 5. Plenum Publishing Corporation.

Dolgobrodov, S; Lukashkin, A.; Russel, I. "Electrostatic interaction between stereocilia: I. Its supporting role in supporting the structure of the hair bundle." Hearing Research. August 2000. 150: 83-93.

Dolgobrodov, S; Lukashkin, A; Russel, I. "Electrostatic interaction between stereocilia: II. Influence on the mechanical properties of the hair bundle." Hearing Research. August 2000. 150: 94-103.

Duncan, RK. (1993) "Finite element analysis of inner ear hair bundles: a parameter study of bundle mechanics." Thesis, Virginia Polytechnic Institute and State University, Blacksburg, VA

Duncan, RK.; Grant, J.W. (1997) "A finite element model of inner ear hair bundle micromechanics". Hearing Research, 104, 15-26.

Eatock, R.A.; Corey, D.P.; Hudspeth, A.J. (1987) "Adaptation of mechanoelectrical transduction in hair cells of the bullfrog's sacculus. J Neurosci 7: 2821-2836

Flock, A. "Electron microscopic and electrophysiological studies on the lateral line canal organ." Acta Oto-Laryngologicia. Supplementum 199. Stockholm, 1965.

Flock, A; Orman, S. (1983)"Micromechanical properties of sensory hairs on receptor cells of the inner ear." Hearing Research, 11: 249-260.

Flock, A.; Strelioff, D. (1984) "Studies on hair cells in isolated coils from the guinea pig cochlea." Hearing Research, 15: 11-18.

Friedmann, Imrich; Ballantyne, John. (1984) Ultrastructural Atlas of the Inner Ear. Butterworths: Boston, MA.

Geisler, D.C. (1988) From Sound to Synapse: Physiology of the Mammalian Ear. New York, NY: Oxford University Press.

Gittes, Mickey F.B., Nettleton, J., and Howard, J. (1993) "Flexural rigidity of microtubules and actin filaments measured from thermal fluctuation in shape." Journal of Cell Biology 120, 923-924.

Goodyear, R.; Richardson, G. (1994) "Differential glycosylation of auditory and vestibular hair bundle proteins revealed by peanut agglutinin." Journal of Comparative Neurology. 345: 267-278.

Holt, J; Corey, D. "Two mechanisms for transducer adaptation in vertebrate hair cells." Proceedings of the National Academy of Sciences. 24 October 2000, 97(22): 11730-11735.

Holt, J.R.; Gillespie, S.K.H.; Provance, D.W. Jr.; Shah, K.; Shokat, K.M.; Corey, D.P.; Mercer, J.A.; Gillespie, P.G. (2002) "A Chemical-Genetic Strategy Implicates Myosin-1c in Adaptation by Hair Cells." Cell. 108 (3): 371-381.

Howard, J; Ashmore, J.F. "Stiffness of sensory hair cell bundles in the sacculus of the frog." Hearing Research, Jan 1986, 23: 93-104.

Howard, J; Hudspeth, A.J. "Mechanical relaxation of the hair bundle mediates adaptation in mechanoelectrical transduction by the bullfrog's saccular hair cell." Proceedings of the National Academy of Sciences. May 1987. 84: 3064-3068.

Howard, J; Hudspeth, A.J. "Compliance of the hair bundle associated with gating of mechanoelectrical transduction channels in the bullfrog's saccular hair cell." Neuron. May 1988, 1: 189-199.

Howard, J; Roberts, W.M; Hudspeth, A.J. (1988) "Mechanoelectrical transduction by hair cells." Ann. Rev. Biophys. Biophys. Chem. 17: 99-124.

Hudspeth, A.J.; Choe, Y; Mehta, A.D.; Martin, P. "Putting ion channels to work: mechanoelectrical transduction, adaption, and amplification by hair cells." Proceedings of the National Academy of Sciences. 24 Oct 2000, 97(22): 11765-11772.

Kachar, B; Parrakkal, M; Zhao, Y; Gillespie, P. "High-resolution structure of hair cell tip links." Proceedings of the National Academy of Sciences. 21 Nov 2000, 97(24): 13336-13341.

Kellermayer, M; Smith, S; Granzier, H; Bustamante, C. "Folding-unfolding transitions in single titin molecules characterized with laser tweezers." Science. 16 May 1997, 276: 1112-1115.

Kelly, James P. (1991) "The Sense of Balance." Principles of Neural Science, 3rd edition. Elsevier Science Publishing Co: New York, NY. pp 500-511.

Langer, M.G; Fink, S.; Koischev, A.; Reshausen, U.; Hordber, J.K.H.; Ruppersberg, J.P. "Lateral mechanical coupling of stereocilia in cochlear hair bundles." Biophysical Journal. Jun 2001, 80: 2608-2621.

Leish, P.R.M; Shepherd, G. M.; Kinnamon, S.C; Santos-Sacchi, J. (1999) "Sensory Transduction." Fundamental Neuroscience. Academic Press: San Diego, CA. pp 703-713.

Lewis, Edwin R; Leverenz, Ellen L; Bialek, William. (1985) The Vertebrate Inner Ear. CRC Press: Boca Raton, FL. pp 17-22.

Merkle, A. (2000) "Implementation of a photoelectronic motion transducer for measuring sub-micrometer displacements of vestibular bundles." Master's thesis, Virginia Tech. Blacksburg, VA.

Neugebauer D.C., Thurm U. "Surface charges of the membrane and cell adhesion substances determine the structural integrity of hair bundles from the inner ear of fish." Cell Tissue Research 249: 199-207. 1987.

Perkins, W.H.; Kent, R.D. Functional Anatomy of Speech, Language, and Hearing. San Diego, CA: College Hill Press, 1986.

Peterson, E. Personal Communication. 2002. Ohio University.

Pickles, J.O.; Cornis, S.D.; Osborne, M.P. "Cross-links between stereocilia in the guinea pig organ of Corti and their possible relation to sensory transduction." Hearing Research, 15: 103-112. 1984.

Pickles, J.O.; Corey, D.P. "Mechanoelectrical transduction by hair cells." Trends in Neuroscience. 1992, 15(7): 254-259

Pickles, J.O. "A model for the mechanics of the stereociliar bundle on acousticolateral hair cells." Hearing Research. Feb 1993, 68: 159-172.

Shepherd, G.M.G.; Corey, D.P. “The extent of adaptation in bullfrog saccular hair cells.” The Journal of Neuroscience. Oct 1994, 14(10): 6217-6229.

Silverman, J.M. (2002) “Experimental measurements of vestibular hair bundle stiffness in the red ear slider turtle utricle.” Master’s thesis, Virginia Polytechnic Institute and State University, Blacksburg, VA.

Szymko, Y; Dimitri, P; Saunders, J. “Stiffness of hair bundles in the chick cochlea.” Hearing Research. Dec 1992, 59: 241-249.

Tilney, Egelman, DeRosier, and Saunders. “Actin Filaments, Stereocilia, and Hair Cells of the Bird Cochlea.” Journal of Cell Biology. Vol 96, March 1983.

Tskhovrebova, L; Trinick, J; Sleep, J.A.; Simmons, R.M. “Elasticity and unfolding of single molecules of the giant muscle protein titin.” Nature. 15 May 1987, 387: 308-312.

Tsuprun, V; Santi, P. “Helical structure of hair cell stereocilia tip links in the chinchilla cochlea.” Journal of the Association for Research in Otolaryngology. 17 Oct 2002. 224-231.

Tsuprun, V; Santi, P. (2002) “Structure of outer hair cell stereocilia side and attachment links in the chinchilla cochlea.” Journal of Histochemistry & Cytochemistry. 50(4): 493-502.

Wersall, J. Bagger-Sjoback, D. (1974) "Morphology of the vestibular sense organ." Handbook of Sensory Physiology. Kornhuber, H.H. Ed., Berlin: Springer-Verlag.

Wilson, Victor; Jones, Geoffrey Melvill. (1979) Mammalian Vestibular Physiology. Plenum Press: New York, NY.

VITA

Joseph Allan Silber was born in Falls Church, Virginia, in February 1979. He spent most of his childhood in Sterling, Virginia, and graduated from the Thomas Jefferson High School for Science and Technology in 1997. In May of 2001, he completed his undergraduate studies at Virginia Tech, receiving his Bachelor of Science in Engineering Science and Mechanics, with a Biomechanics concentration and a minor in Mathematics. Joseph married Deborah Freshwater in June 2002. In addition to his academic studies, Joseph enjoys reading, movies, music, and hiking.